MODE MIXING IN STEP INDEX MULTIMODE FIBRE

Gerard Shaw, B.Sc. (Applied Physics)

A thesis submitted to Dublin City University in candidacy for the degree of Master of Science.

August 1993

I hereby declare that none of the material contained in this thesis has been used in any other submission for any other award. Further that the contents of this thesis are the sole work of the author except where an acknowledgement has been made for any assistance received.

Supervisor: Dr. Vincent Ruddy
School of Physical Sciences
Dublin City University

DECLARATION

I hereby certify that this material, which I now submit for assessment on the programme of study leading to the award of Master of Science, is entirely my own work and has not been taken from the work of others save and to the extent that such work has been cited and acknowledged within the text of my work.

Signed: Gerard Shaw. **Date:** 17/9/93

Candidate.

TABLE OF CONTENTS.

LIST OF FIGURES i

ABSTRACT iv

ACKNOWLEDGEMENTS v

DEDICATION vi

CHAPTER 1: EVANESCENT WAVE SPECTROSCOPY

1.1 INTRODUCTION 1

1.2 THE EVANESCENT WAVE 1

1.3 MODAL DEPENDANCE OF PENETRATION DEPTH 2

1.4 EFFECTIVE ATTENUATION COEFFICIENTS 6

1.5 MODAL PERTURBATIONS 7

1.6 FIBRE EVANESCENT WAVE SENSORS/ FIBRE CONSIDERATIONS 8

REFERENCES (CHAPTER 1) 10

CHAPTER 2 MODAL ANALYSIS - EXPERIMENTAL SYSTEM

2.1 INTRODUCTION 11

2.2 FIBRE LIGHT LAUNCHING RIG 11

2.3 FIBRE END PREPARATION 13

2.4 MODAL DETECTION SYSTEM 14

2.5 CONCLUSIONS 17

CHAPTER 3 MODAL ANALYSIS - DATA ACQUISITION

3.1 INTRODUCTION 18

3.2 CAMERA SOFTWARE 18

3.3 NEAR FIELD INTENSITY PROFILES 20

3.4 IMAGE ANALYSIS SOFTWARE 22

3.5 CONCLUSIONS 24

CHAPTER 4 MODAL ANALYSIS

4.1 INTRODUCTION 26

4.2 EXPERIMENTAL DATA 26

4.3 MODE COUPLING THEORIES 34

4.4 THE ANGLE INDEPENDENT COUPLING MODEL 37

4.5 DIFFUSION WITH AN INVERSE θ^2 DEPENDENCE OF COUPLING COEFFICIENT 43

4.6 COMPARISON WITH OTHER MEASUREMANTS 47

4.7 SIGNIFICANCE OF MODAL COUPLING IN EVANESCENT WAVE SENSING 48

4.8 CONCLUSIONS 50

REFERENCES (CHAPTER 4) 51

APPENDIX 1 THE I-SCAN LINEAR ARRAY SYSTEM 53

APPENDIX 2 SOFTWARE PROGRAMS 98

LIST OF FIGURES

FIGURE 1 BOUND MODES (RAYS) AND THEIR EVANESCENT COUNTERPARTS IN AN OPTICAL FIBRE. 3

FIGURE 2 BASIC PRINCIPLE OF EVANESCENT WAVE SPECTROSCOPY USING A MULTIMODE FIBRE. 5

FIGURE 3 (A) LAUNCH OPTICS 12
(B) RAY PATHS ENTERING, TRANSMITTED BY, AND EXITING THE FIBRE.

FIGURE 4 SYSTEM USED TO MEASURE MODAL DIFFUSION IN FIBRE. 15

FIGURE 5 A SAMPLE OF THE OUTPUT OF ONE SCAN USING THE LINEAR CCD ARRAY. 16

FIGURE 6 (A) MODAL POWER DISTRIBUTION ON CAMERA. 19
(B) POWER PATTERN AS A FUNCTION OF θ AND r.

FIGURE 7 RAY OPTICS TO CAMERA. 21

FIGURE 8 AN EXAMPLE OF AN INTENSITY vs AXIAL ANGLE PROFILE DISPLAYING HALF POWER VALUE. 25

FIGURE 9 ANGLE DEFINITIONS WITHIN FIBRE. 27

FIGURE 10 EXPERIMENTAL VARIATION OF ϕ WITH z; NA = 0.25 LAUNCH OBJECTIVE. 29

FIGURE 11 VARIATION OF ϕ^4WITH z; NA = 0.25 LAUNCH OBJECTIVE. 30

FIGURE 12 EXPERIMENTAL VARIATION OF ϕ WITH z; NA = 0.4 LAUNCH OBJECTIVE. 31

FIGURE 13 VARIATION OF ϕ^4WITH z; NA = 0.4 LAUNCH OBJECTIVE. 32

FIGURE 14 VARIATION OF A_N VERSUS n FOR FOURIER BESSEL EXPANSION. 40

FIGURE 15 SCHEMATIC OF PULSE BROADENING DUE TO DIFFUSION. 41

FIGURE 16 GLOGE MODEL, PULSE BROADENING AS A FUNCTION OF NORMALISED DISTANCE 42

FIGURE 17 ANGLE DEPENDENT COUPLING MODEL - VARIATION OF ϕ WITH LENGTH. 45

FIGURE 18 BROADENING OF SQUARE WAVE PULSE WITH DISTANCE, ALL CURVES ARE NORMALISED W.R.T. P_{MAX} 46

ABSTRACT

The presence of optical radiation outside the core of a step index fibre - the so called evanescent wave - offers a technique for chemical sensing by attenuated total interval reflection spectroscopy (ATR). The penetration of the evanescent wave power in the sensing region is dependent upon the modal structure in the fibre core. In this thesis a method for measuring the variation of modal power distribution with distance along the fibre using a CCD camera is described and used for large diameter plastic clad silica fibre (PCS). Both linear and two dimensional array cameras are used to profile the optical power distribution in the fibre core and the results obtained are discussed in terms of diffusion models. The suitability of such fibre for ATR spectroscopy is evaluated in light of the experimental results.

ACKNOWLEDGEMENTS

Firstly I must pay tribute to my supervisor, Dr. Vincent Ruddy for his unending interest and giudance during this project. Thanks also to the other members of the academic staff of the School of Physical Sciences, in particular Brian MacCraith and Brian Lawless. I must also thank the technicians, especially Alan Hughes, Joe Maxwell and Al Devine, and the secretarial staff.

Thanks to my colleagues in the various research groups in the physics department and particularly in the sensors group for their assistance and good humour. Thanks to Kieran O'Dwyer and Cait O'Byrne for their help with software, to Valerie for typing and to Eamonn and Cormac for the use of facilities. Last but by no means least, I would like to express my gratitude to Amdahl Ireland Ltd. for their support through their Educational Assistance Programme.

DEDICATION

THIS THESIS IS DEDICATED TO VALERIE FOR HER ASSISTANCE, ENCOURAGEMENT AND COMPANIONSHIP, TO CONALL FOR ENRICHING MY LIFE AND ALSO TO LORCAN AND ANNE FOR GIVING ME A GOOD HEAD START.

CHAPTER 1.

EVANESCENT WAVE SECTROSCOPY.

1.1 INTRODUCTION.

The detection of chemical species by attenuation of optical power at a characteristic (or analytical) wavelength is the basis of absorption spectroscopy. When the detection technique is based upon the attenuation of the evanescent wave associated with total internal reflection at the interface between two media the technique is called ATR - Attenuated Total Reflection or Evanescent Wave Spectroscopy. In this chapter the evanescent wave in a planar and cylindrical waveguide is discussed, the penetration depth defined and the parameters that determine the strength of the absorption process are described. The analysis is developed in the context of multimode step index fibre waveguides.

1.2 THE EVANESCENT WAVE.

At the interface of two media (of refractive indices n_1 and n_2) total internal reflection of light occurs for light incident (at the higher index side) at angles greater than $\mathrm{Sin}^{-1}\, n_2/n_1$. Associated with this total internal reflection is an evanescent wave in the lower index medium which

(i) Propagates along the interface,

(ii) Decays exponentially in amplitude perpendicular to the interface [Ref 1] with a penetration or 1/e depth of

$$\frac{\lambda}{2\pi n_1\sqrt{\sin^2\theta-(n_2/n_1)^2}} \qquad 1.2.1$$

as shown in Fig. 1. λ is the free space or vacuum wavelength and θ the incident angle with respect to the interface normal.

1.3 MODAL DEPENDENCE OF PENETRATION DEPTH.

The situation displayed in Figure 1 pertains to a planar interface. For a cylindrical waveguide of step index variety the allowed solutions of the wave equation specify each ray in terms of core and cladding parameters U and W defined by

$$U=a\sqrt{n_1^2k^2-\beta^2} \qquad W=a\sqrt{\beta^2-n_2^2k^2} \qquad 1.3.1$$

for radiation of free space wavenumber $k = 2\pi/\lambda$ and propagation constant ß. The core radius is a. ß represents the component of the wave vector n_1k along the direction of propagation, i.e.

$$\beta=n_1kCos\theta_z \qquad 1.3.2$$

where θ_z is the angle the ray makes with the axis of the fibre [Ref 2]. θ_z and θ of Eqn 1.2.1 are complementary. The matching of the E field and its derivatives at the interface gives rise to an eigenvalue equation. The solutions of this equation provide a set of permitted values of ß corresponding to a set of modes in the fibre. When the fibre is large in diameter ($a >> \lambda$) the various values of ß are close together and the fibre normalised frequency, or V number, defined by

$$V=\frac{2\pi a}{\lambda}\sqrt{n_1^2-n_2^2} \qquad 1.3.3$$

is also large. V is also given by

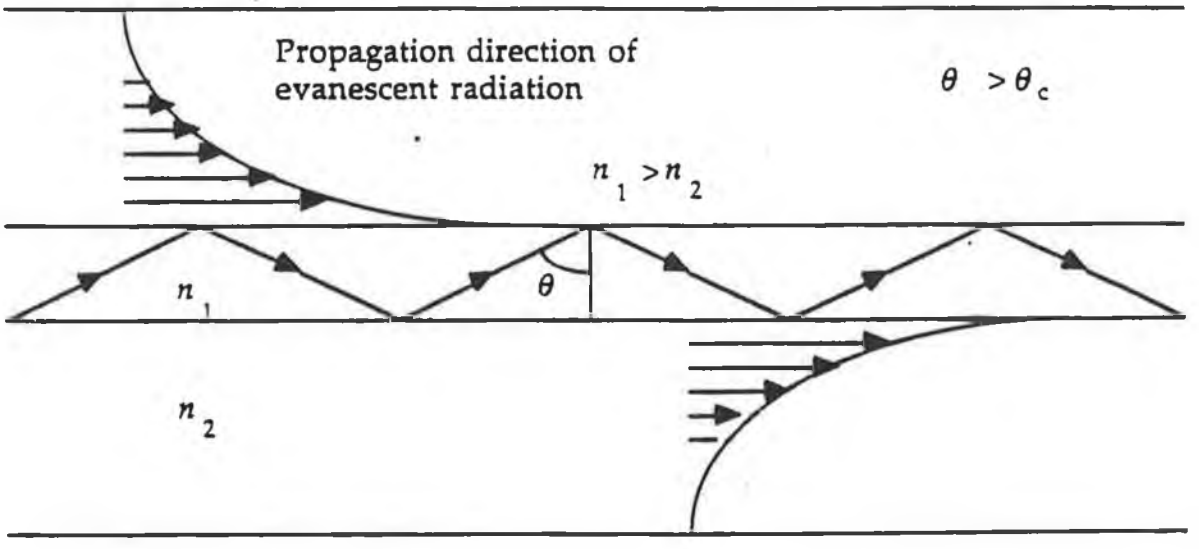

FIGURE 1: BOUND MODES (RAYS) AND THEIR EVANESCENT COUNTERPART IN AN OPTICAL FIBRE.

$$V^2=U^2+W^2 \qquad 1.3.4$$

The cladding parameter W determines the penetration depth of the field of the mode in the cladding as the field can be expressed in terms of a modified Bessel function $K_l(Wr/a)$ where r is distance from the fibre axis. The modified Bessel function can, in the limit of large W, be expressed as an exponential giving rise to a E field penetration depth (or 1/e depth) of

$$\frac{a}{W} \qquad 1.3.5$$

which reduces to the expression given in 1.2.1. It can be seen from 1.3.5 that as W -> 0 the field penetration depth in the cladding increases, becoming infinite at W = 0. W = 0 is called mode cut off. Modes with small values of W (i.e. modes close to cut off) are rays with incident angles close to the critial angle. These are termed high order modes. The ray direction corresponds to the maximum value of θ_z. Modes with large values of W (or U value close to V) are termed low order modes and are associated with rays travelling almost parallel to the fibre axis (values of θ_z close to zero).

In evanescent wave or ATR spectroscopy using a multimode fibre as the sensing probe - see Figure 2 - it is important then to know the values of W of the modes present in the sensing region and to have as many high order modes (with corresponding large penetration depth) as possible. This thesis describes how the modal pattern may be measured experimentally for evanescent wave spectroscopy applications.

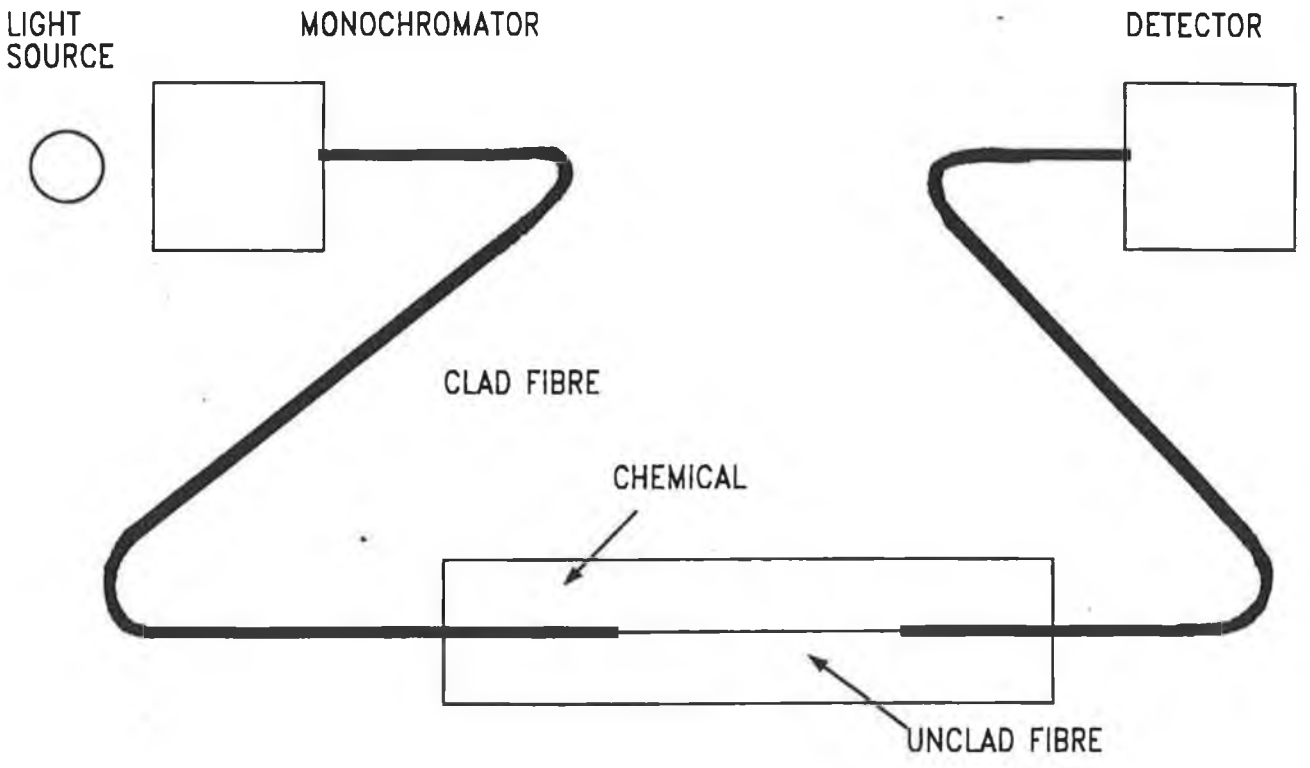

FIGURE 2: BASIC PRINCIPLE OF EVANESCENT WAVE SPECTROSCOPY USING A MULTIMODE FIBRE.

1.4 EFFECTIVE ATTENUATION COEFFICIENT.

In simple transmission spectroscopy the transmitted beam intensity I is related to the incident intensity I_0 by the Beer - Lambert Law

$$I=I_0\exp(-\epsilon bc) \qquad 1.4.1$$

where ϵ = species absorptivity at an analytical wavelength

b = path lengh of light beam in sample

c = sample concentration.

The absorbance A of the sample defined as $\log_{10}(I_0/I)$ is then linearly dependent on

(i) absorptivity

(ii) path length

(iii) sample concentration

In ATR, or evanescent wave spectroscopy using a fibre, the transmitted intensity depends upon

(a) the length of fibre exposed to the chemical Z [the equivalent of b in Eqn 1.4.1]

(b) the absorptivity of the chemical (at the analytical wavelength) [as in Eqn 1.4.1]

(c) the sample concentration [as in Eqn 1.4.1]

(d) the fraction (f) of the optical power that exists in the lower index medium. [This parameter is particular to fibre ATR] This is discussed in [Ref 8].

The value of f depends critially on the optical modes available at the sensing section of the fibre and their closeness to cut off. In the case where all the possible bound modes of the fibre - all $V^2/2$ of them - are available for sensing the

value of f is $4\sqrt{2}/3V$ as derived by Gloge [Ref 3]. Thus for large diameter fibres the fraction f is small. Where only a selection of all the possible bound modes is used (the other being removed for example by spatial filtering) the value of f can be calculated from an expression of Ruddy [Ref 4]. The removal of lower order modes - by spatial filtering or otherwise - enhances the sensitivity of the such sensors as shown by some authors [Ref 5,6,7,].

1.5 MODAL PERTURBATIONS.

In a perfect cylindrical waveguide a bound mode (having a particular value of ß, represented by a ray which always crosses the fibre axis with the same angle) propagates indefinitely without perturbation or attenuation. This assures that the ray

(i) meets no scattering centre in the fibre core.

(ii) is completely reflected at each turning point at the core / cladding interface, i.e. is not scattered to a different reflection angle at any reflection.

The fact that a fibre has a finite attenuation coefficient over a large range of wavelengths means that as well as absorption due to impurities in the core and cladding materials there are also losses due to scattering of the light by imperfections in the core material, imperfections at the interface between core and cladding and impurities and imperfections in the cladding. These imperfections may result in modes being perturbed and nearest - neighbour coupling, where power contained in lower order modes is transfered to higher - order modes and visa versa gives rise to a intermodal dispersion that varies as $Z^{1/2}$ as distinct from Z as predicted by ray optics. [Refs 9,10] Z is distance along

the fibre. Power carried by higher order modes (close to cut off) may be transferred to radiation modes which propagate energy into the cladding and as a result reduces the bound mode power in the core.

Intermodal coupling has been examined by Gloge [Ref 11] who treated the problem as one of diffusion between closely adjacent modes. Being a diffusion type process the intermodal coupling will distribute power evenly in the fibre (with the exception of the highest order modes which lose power at a higher rate to radiation modes than can be supplies by their neighbours).

1.6 FIBRE EVANESCENT WAVE SENSORS / FIBRE CONSIDERATIONS.

For evanescent wave sensing the fibre cladding must either be permeable to the chemical being analysed or removeable so that the evanescent wave power can access the chemical in a sensing zone. In the case of gas sensors a porous polymer clad glass core fibre may be used as described in [Ref 6,12]. Such a fibre having an interface between glass and a plastic is expected to have considerable scattering at this interface and as a result a substantial degree of mode mixing. Where the polymer cladding of a PCS (plastic clad silica) fibre is removed to allow the evanescent power access to a chemical in which the fibre is located a knowledge of the modal power distribution coming into the sensing region is required in order to relate the measured absorbance to the concentration of the species. While plastic clad fibre then is particularly suitable for evanescent wave absorption spectroscopy of chemicals the modal power

distribution within the core is a prerequisite to quantitative chemical analysis. This thesis describes how the modal power distribution in such a multimode step index PCS fibre is measured.

REFERENCES (Chapter 1)

1. N.J. Harrick " Internal Reflecton Spectroscopy"
   (Harrick Scientific Corp. N.Y. 1987)
2. A.W.Snyder, J.D. Love "Optical Waveguide Theory",
   (Chapman & Hall 1983)
3. D. Gloge Appl. Opt. 10 2252 (1971)
4. V. Ruddy Fibre & Integrated Optics 9 142 (1990)
5. S. Simhony, A. Katzir, E.M. Kosower. Anal. Chem. 60 1908 (1988)
6. V. Ruddy, S. Mc Cabe & B. Mac Craith
   Appl. Spectros. 44 (9) 1461 (1990)
7. B. Mac Craith, V. Ruddy, C. Potter, B. O Kelly, J. Mc Gilp
   Electron. Lett 27 (14) 1247 (1991)
8. V. Ruddy, B.D. Mac Craith & J.A. Murphy
   J. Appl. Phys 67 (10) 6070 (1990)
9. Ref. 2 above Section 5-22 p. 116.
10. D. Marcuse "Theory of Dielectric Optical Waveguides"
    (Academic Press N.Y. 1974) p.213 Eqn 5.5.68
11. D. Gloge Bell Syst. Tech. J. 6 801 (1973)
12. V. Ruddy, K. Lardner Int. J. Optoelectronics 8 (1) 87, (1993)

CHAPTER 2

MODAL ANALYSIS - EXPERIMENTAL SYSTEM.

2.1 INTRODUCTION.

In this chapter the optical systems used (i) to launch bound modes into plastic clad silica (PCS) fibre and (ii) to detect the modal pattern at various cut-back lengths of the fibre are discussed. Linear and two dimensional CCD detector arrays are discussed and the fibre end preparation process is described.

2.2 FIBRE LIGHT LAUNCHING RIG.

To launch a particular set of modes into the fibre a microscope objective, visible LED at the focal point of a collimating lens, and annular mask were used as shown in Figure 3A. The numerical aperture of the microscope objective together with the annular radii of the mask determine the range of launch angles of the light into the fibre core. Figure 3B shows the rays paths to, in and from the fibre. A range of microscope objectives of numerical aperture

0.25

0.40

0.85

was used. The numerical aperture of the fibre used is given as 0.4 at the wavelength of the source used (a red LED of peak wavelength 635 nm). The range of objectives used covered underfilling, filling and overfilling the entrance acceptance cone of the fibre (given as a half angle of Sin^{-1} 0.4 or 23.58°).

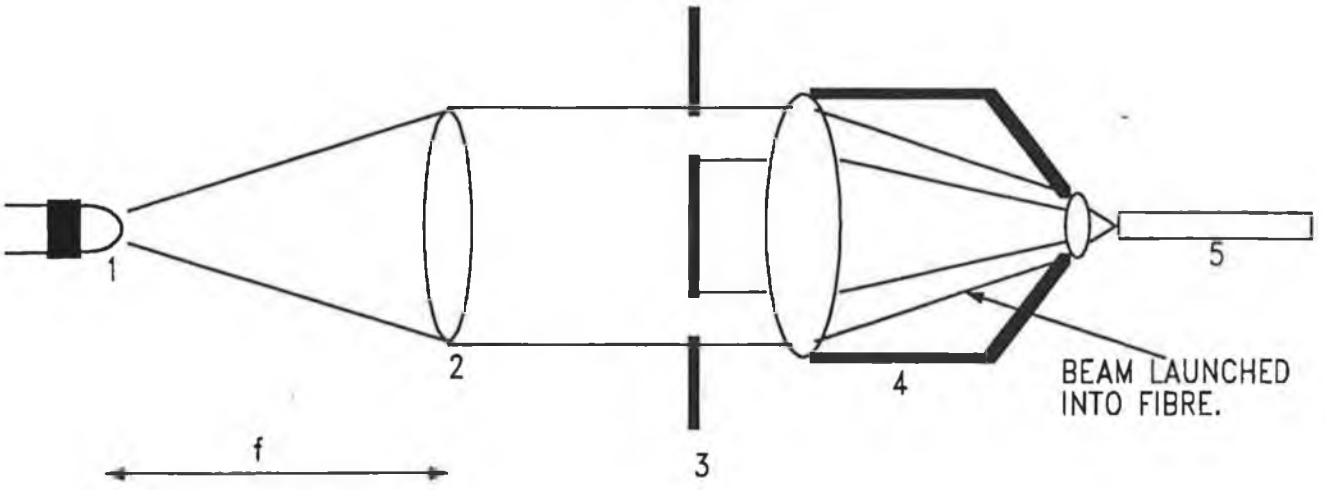

FIGURE 3A : LAUNCH OPTICS

1 = LED 2 = LENS

3 = ANNULAR BEAM MASK

4 = MICROSCOPE OBJECTIVE

5 = FIBRE (LOCATED IN BRASS FIBRE CHUCK).

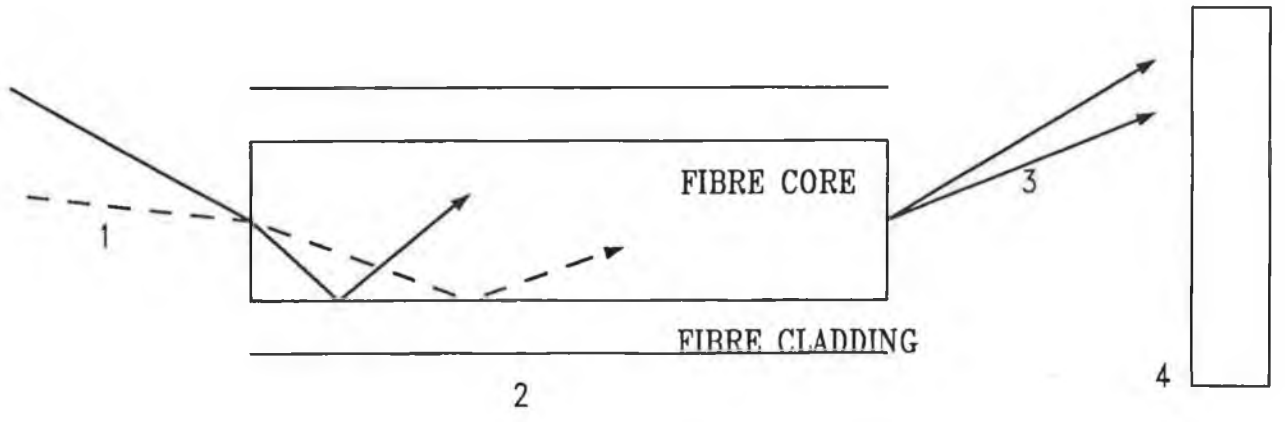

FIGURE 3B: RAY PATHS ENTERING, TRANSMITTED BY AND EXITING THE FIBRE.

1 = INCIDENT LIGHT CONE FROM MICROSCOPE OBJECTIVE.

2 = MULTIMODE STEP INDEX FIBRE.

3 = EXITING LIGHT CONE.

4 = DETECTOR ARRAY.

2.3 FIBRE END PREPARATION.

The launch end of the fibre was prepared by cleaving the fibre, securing it in a chuck with wax and placing this chuck (together with some dummy chucks for balance) in a Fibre Tree for polishing on a Logitech PM2A Precision Lapping Machine. Fused Aluminium Oxide polishing abrasive of grit size 9 microns and finally 3 microns on a cast iron lapping plate and finally on an expanded polyurethane polishing plate was used. The end face was inspected regularly with a high magnification microscope for surface quality. The launch end was not modified in any way during the course of the modal analysis.

The distal end was cleaved, polished on a series of increasingly finer polishing cloths in a figure 8 configuration. For this process the fibre was held in a brass chuck and systematically inspected as before for quality of the polished surface.

A spool of 35m of 600 micron diameter core PCS fibre was used, examined for modal distribution using the 3 microscope objectives in sequence, then cut-back by 1 metre and the process repeated. A series of data files of modal pattern as a function of fibre length and launch numerical aperture (0.25, 0.40 or 0.85) was then prepared.

To remove cladding modes that may inadvertedly be launched the fibre was surrounded by a glycerin impregnated sponge. No red glow was observed indicating that cladding modes were not launched into the

fibre in any substantial quantity, (the source used was red LED).

2.4 MODAL DETECTION SYSTEMS.

The modal pattern in the fibre at a distance Z (from the launch end) was investigated by allowing the light coming from the fibre to fall on a linear and two dimensional array of CCD (charge coupled device) detectors, as shown in Figure 4. Initially a linear array of 256 elements - a Fairchild CCD 111 chip was used and a circuit designed, fabricated and tested to output the linear array, as a series of discrete dc voltage levels, onto a chart recorder. A full description of the electronics is given in Appendix 1.

A plot of one scan of the light pattern is shown in Figure 5. The spread in the modal power is one dimension (x in diagram) can be seen.

It was found that the linear array system had several restrictions. It was difficult to position the fibre such that the light emitted was centred over the array. It was not sensitive enough to detect small variations in modal power distribution. Also comparision of hard copies of graphed data is not a satisfactory means of comparing the differences between scans recorded under different conditions. A 2 dimensional CCD camera system - which facilitated a complete mapping of the modal power distribution - was thought to be more suitable.

At the time of writing we became aware of similar work by Norris and Smith [Ref. 24]. With a linear array (Oriel Intraspec 512 pixel

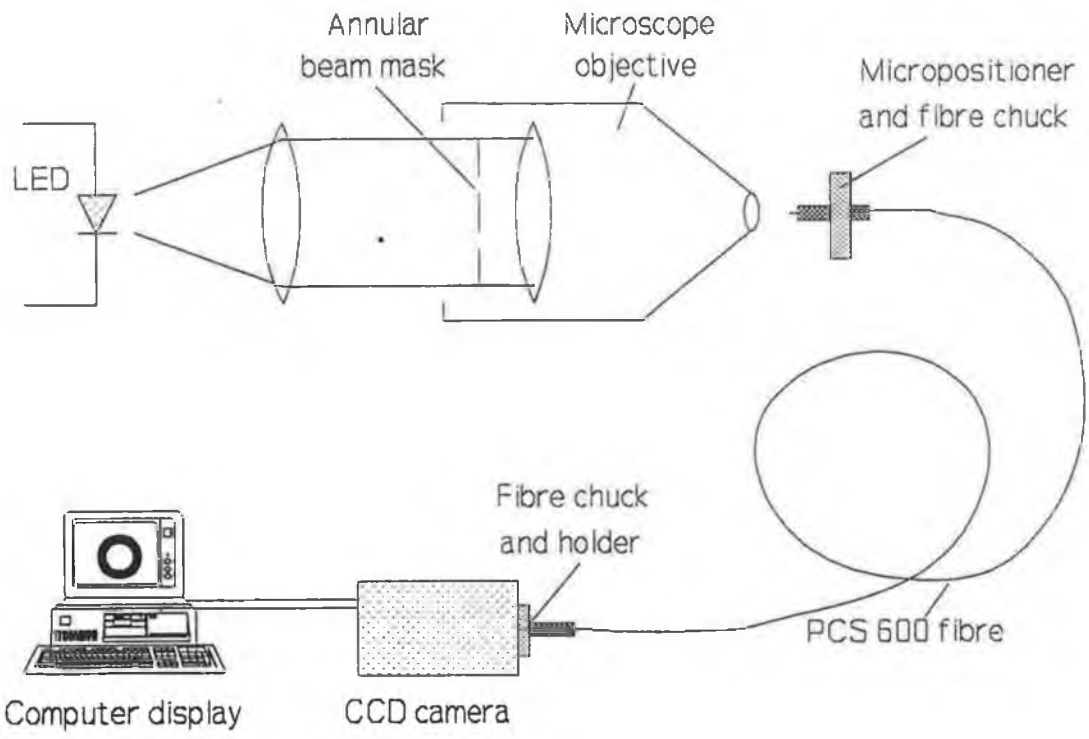

FIGURE 4: SYSTEM USED TO MEASURE MODAL DIFFUSION IN FIBRE.

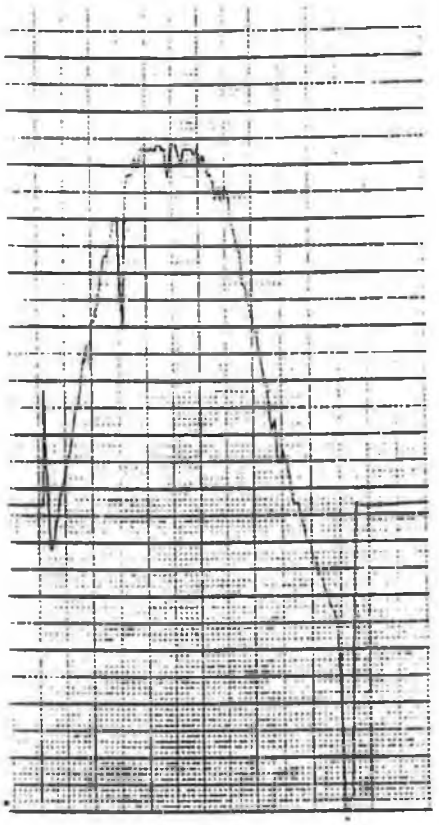

A SAMPLE PLOT FROM THE
1 DIMENSIONAL ARRAY

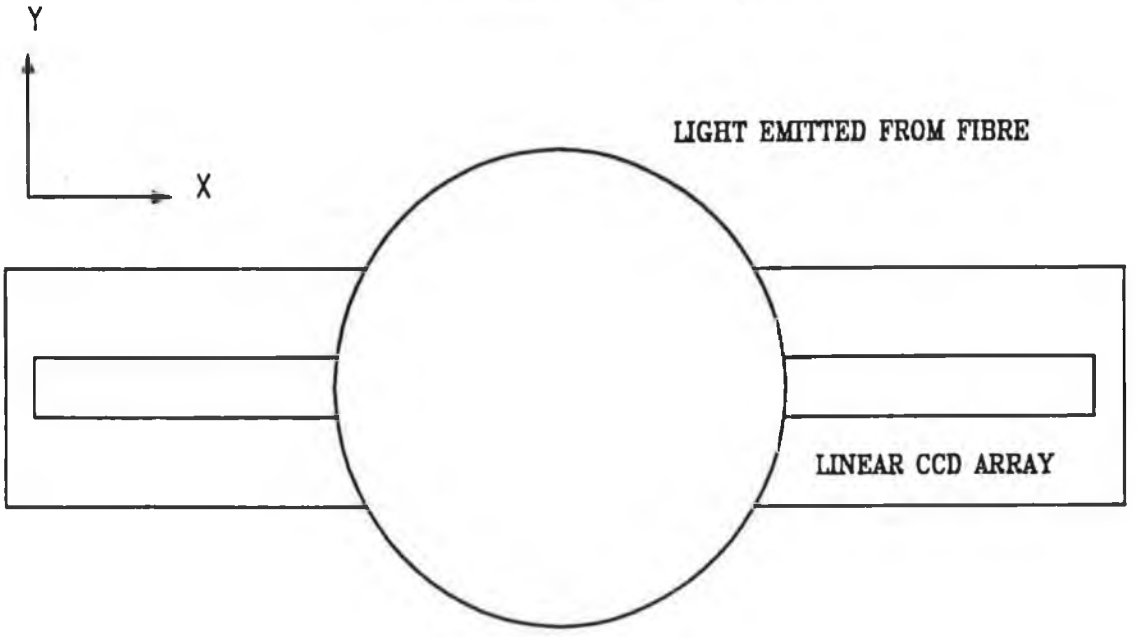

FIGURE 5: A SAMPLE OF THE OUTPUT FOR ONE SCAN USING THE LINEAR CCD ARRAY.

device) they experienced difficulties in observing mode coupling in fibres as well. Unlike this work they made no measurements with 2 dimensional detector arrays.

An Electrim Corporation EDC-1000 with a pixel array of 192 (H) x 165(V) elements, complete with IPS (Image Processing Software) version 1.0 from Mnemonics Inc. was used. The pixels had a spectral range of 400 - 1100 nm with a peak quantum efficiency at 700nm close to that of the red LED used as a light source. The camera system is powered by a multiconductor cable from a computer, see photograph 1. The camera output system is an 8 bit digital signal corresponding to a brightness which has 256 grey levels. Software packages used to process the image are discussed in Chapter 3.

At each measurement the distal end of the fibre was loaded into a brass fibre chuck with the fibre tip just proud of the chuck. The chuck was then inserted into a guiding sleeve fabricated for the camera head and inserted gently until the fibre touched the face of the CCD array. Then the chuck was locked in place using a grub screw.

2.5 CONCLUSION.

The optical system used to set up a particular modal pattern in the fibre and analyse the transmitted modal pattern as a function of both fibre length and launch numerical aperture has been discussed. The data obtained and its analysis in terms of modal diffusion will be discussed the the next two chapters.

PHOTOGRAPH 1A: THE ELECTRIM CORPROATION EDC-1000 CAMERA USED TO CAPTURE IMAGES.

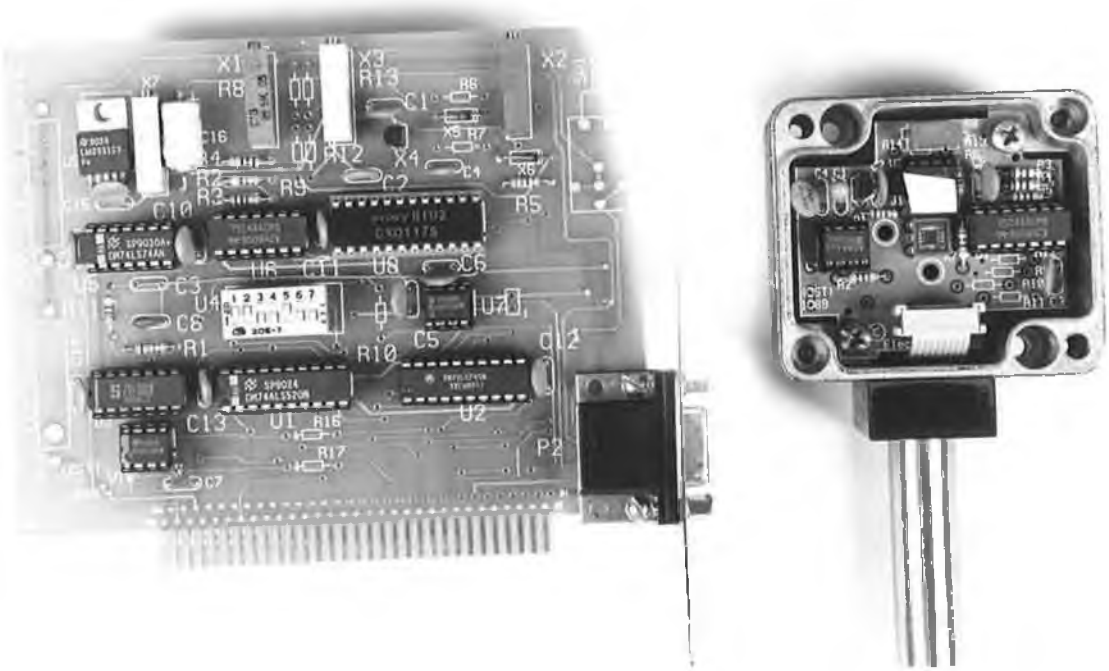

PHOTOGRAPH 1B: DETAILED SHOT OF CAMERA CIRCUIT.

CHAPTER 3.

MODAL ANALYSIS - DATA ACQUISITION.

3.1 INTRODUCTION.

The capture of light intensity profiles at the distal end of the fibre is discussed and the software used to determine the modal power distribution as a function of radius r on the pixel array of the camera is described. The radius r is a direct measure of the angle θ since $\tan \theta = r/x$, where x is the distance from the fibre end face to the pixel active surface, (See Figure 6). Modal Power Distributions are shown for constant launch NA as a function of fibre length Z. Patterns for 3 different launch numerical aperture, corresponding to underfilling, filling and overfilling the entrance cone of the fibre are displayed.

3.2 CAMERA SOFTWARE.

The ELECTRIM CORPORATION EDC - 1000 Two Dimensional CCD Camera was used in conjunction with IPS, Image Processing Software, Version 1.0 from MNEMONICS INCORPORATED. The IPS package was used to display a live image of the intensity profile at the distal end of the fibre, adjust sensitivities, enhance images etc... and to save a data file to disk in a .BUF format. The file could be retrieved for further processing using this software.

Each intensity profile, for a particular launch NA and fibre

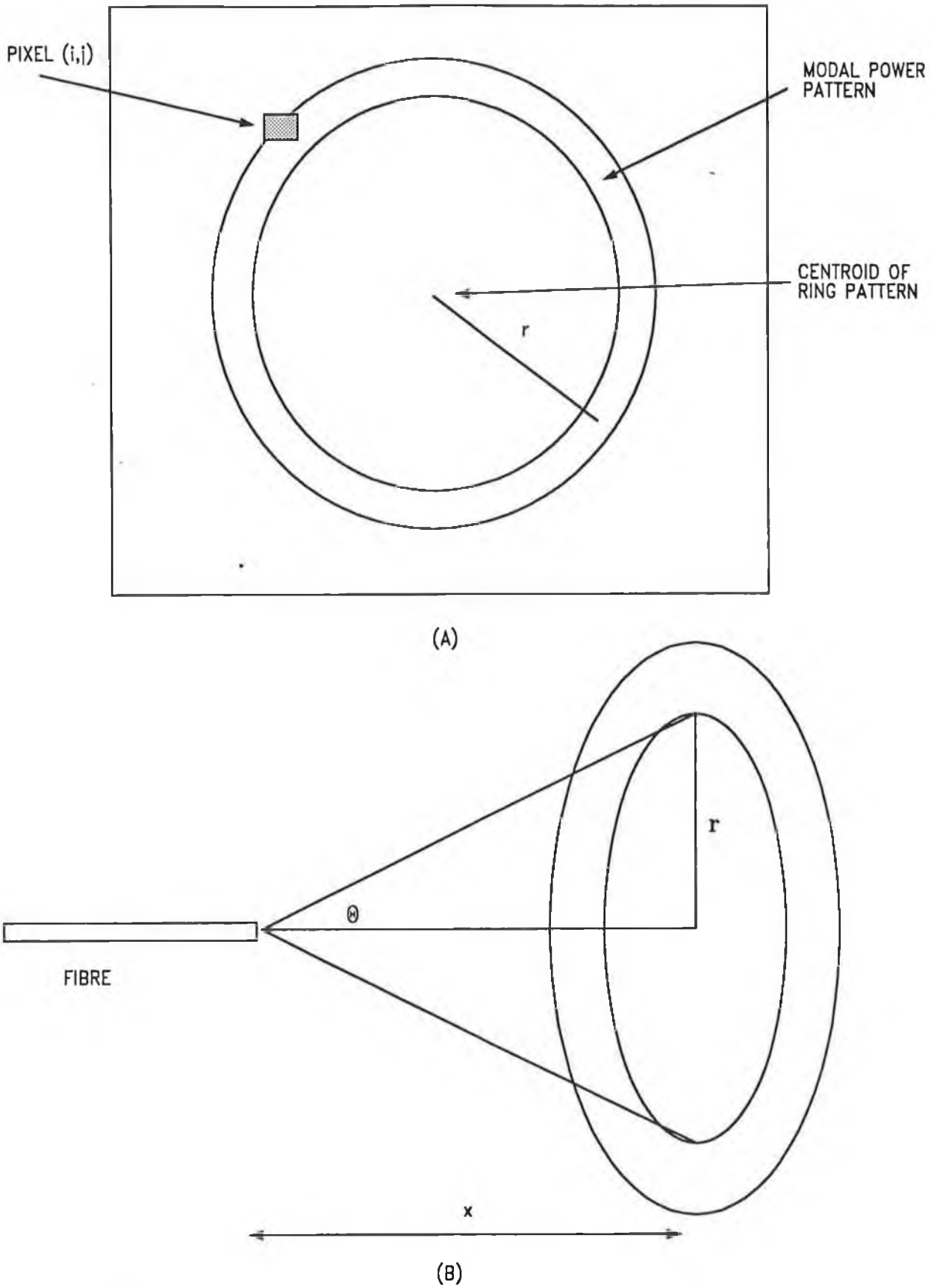

FIGURE 6: (A) MODAL POWER DISTRIBUTION ON CAMERA.

(B) POWER PATTERN AS A FUNCTION OF θ AND r.

length Z, represents a 192x165 array of numbers in the range 0-256 (2^8 for 8 bit). The frame is grabbed using an IPS option and stored as a data file with a name such as L20NA1A.BUF representing the launch NA and the order of the cut back (L) (for example, cut back 20 corresponds to a fibre length y = 35 - 20 = 15 metres). Several images were recorded in each case (A,B,C...). A software package called CENTRE.C (listed in Appendix II) was written to determine the centroid (Xc,Yc) of the pattern. Xc and Yc represent pixel locations of the centroid. The CENTRE. C program was further developed as follows:
Using the centriod (Xc,Yc) each pixel within an annulus defined by the radii r_1 and r_2 was interograted and the integrated intensity in the annular band computed. The results were plotted on screen and stored to a file. The resultant program was called ANALYSE2.C (See Appendix II).

3.3 NEAR FIELD INTENSITY PROFILES.

As stated earlier the near field optical power intensity pattern was imaged on a CCD camera as a annulus of light. Data files of the pattern as a function of

(i) launch optics numerical aperture

(ii) fibre length Z

were recorded on disk. At small values of Z (the fibre length) the annulus was well defined (for a particular launch objective). As Z increased the annulus became more diffused indicating a coupling of the many optical modes to higher and lower meridioanal angles θ (See Figure 7). The fibre ray angle θ is related

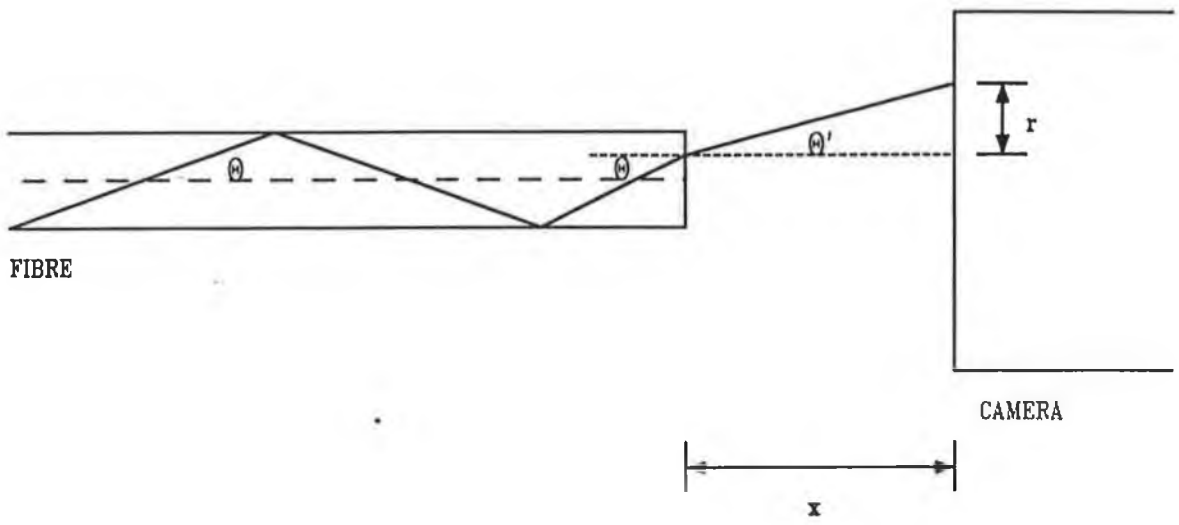

$$\theta \approx Sin\theta = \frac{1}{n} Sin\theta' = \frac{r}{nx}$$

FIGURE 7: RAY OPTICS TO CAMERA.

The distance x (the displacement of the active surface of the CCD array from the fibre face) is exaggerated. n is the fibre core refractive index.

ar ring on the CCD by the expression

$$\theta=\frac{r}{nx} \qquad 3.3.1$$

ation, where n is the core refractive index of the silica
of the fibre from the active surface of the CCD array
e apparent thickness of this plate was measured with
e 1000 μm. Taking a refractive index of 1.5 for the
ming it is crown silica) the actual plate thickness is
1.5 mm

AXIAL ANGLE

$$x=1.5mm \qquad 3.3.2$$

)m a pixel distance of q pixels to a physical distance
6 μm per pixel so that

$$\frac{q(16X10^{-6})}{46)(1.5X10^{-3})} = 7.31X10^{-3}q \qquad 3.3.3$$

ians. The refractive index of silica is taken as 1.46.
am can then be seen as a variation in the parameter
a variation in θ using 3.3.3.

NGLE

)FTWARE.

age analysis software used was written to execute the

co-ordinates of the centre of the

CHAPTER 4.

MODAL ANALYSIS

4.1 INTRODUCTION

The variation of the modal power distribution $P(\theta)$ with distance z along the fibre as measured experimentally is compared with a diffusion model of Gloge [19]. A diffusion or coupling coefficient between modes for the fibre used - plastic clad silica fibre of core diameter 600μm - is calculated and compared with published data for other types of fibre. The experimental data is found to follow a modal power broadening which scales as $z^{1/4}$ which is consistent with a mode coupling coefficient which varies as $(\theta_c/\theta)^2$.

The importance of modal diffusion to evanescent wave sensing is then discussed. [θ and θ_c are internal angles of the light rays within the fibre as shown in Fig 9]

4.2 EXPERIMENTAL DATA.

Using a launch objective of NA = 0.25, with the near axial radiation blocked out by an opaque mask, light was launched into the fibre (of NA = 0.4). Such a system launches a beam of constant power density in the angular zone

$$\theta_1 \leq \theta \leq \theta_2 \qquad 4.2.1$$

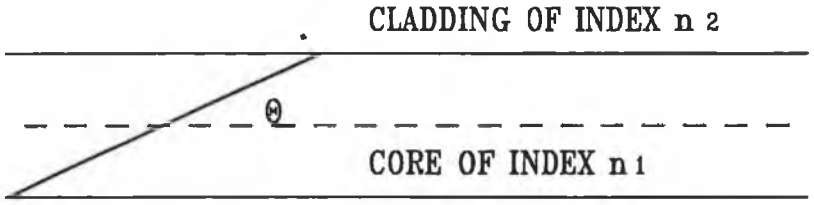

FIBRE

FIG 9: ANGLE DEFINITIONS WITHIN FIBRE.

θc IS THE MAX VALUE OF θ AND GIVEN BY

$$\theta_c = Cos^{-1}\, n_2/n_1$$

n_1 AND n_2 ARE CORE AND CLADDING INDICES RESPECTIVELY.

where θ_1 is determined by the radius of the opaque mask and θ_2 by the numerical aperture (NA) of the launch objective ($\theta_2 = \mathrm{Sin}^{-1}$ NA). Thus at the launch end (z=0) an angular cone of light is transmitted into the fibre. The angular spreading of this beam with distance z along the fibre is then a measure of the the coupling between modes. When projected onto the camera face at the distal end the location of the half power point radii q (ie a pixel location index) is converted to a half power angle ϕ as discussed in Section 3.2.

Table 1 shows the calculated values of the half power axial angle ϕ (within the fibre) expressed in radians as a function of the fibre length z for an NA=0.25 launch objective.

TABLE 1

z(meters)	1	3	6	14	21
q	8.5	10.0	12.0	15.0	18.5
ϕ(rad)	0.1359	0.1601	0.1920	0.2400	0.2639

The variation of ϕ with fibre length z is shown in Fig 10.

In Fig 11 the variation of ϕ^4 with z is shown. The linear dependence of ϕ, the beam divergence, on $z^{1/4}$ is thus demonstrated. We will see how these results can be reconciled with a particular type of diffusion or mode coupling model.

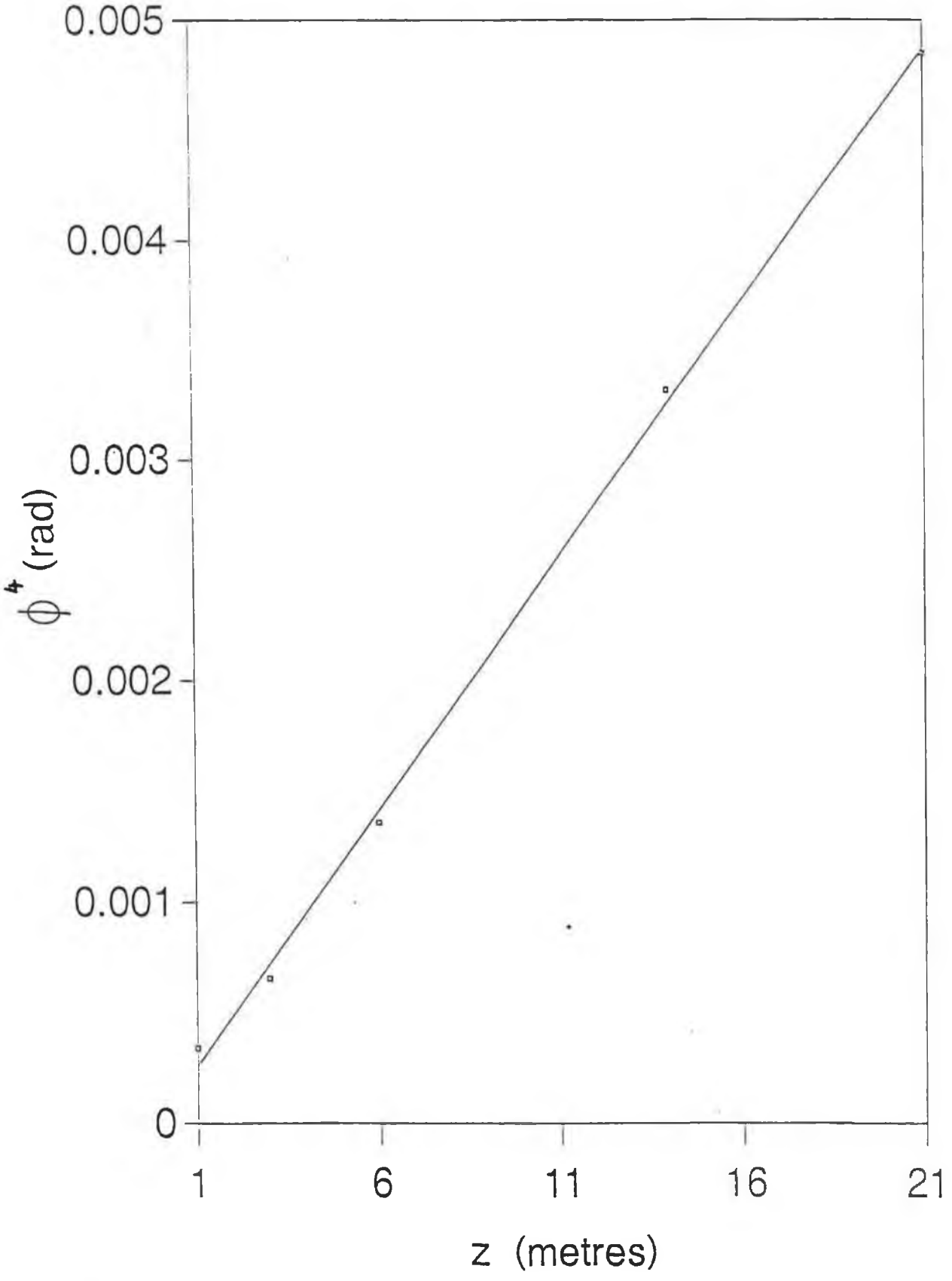

FIGURE 11: EXPERIMENTAL VARIATION OF ϕ_4 WITH z; NA = 0.25 LAUNCH OBJECTIVE.

When higher order modes are launched with an objective of NA = 0.4 - again with an axis beam mask to remove low order modes - a similar linear dependence of ϕ on $z^{1/4}$ is observed. See Table 2 and graphs Fig 12 and Fig 13. (The values listed for ϕ represent angles internal to the fibre.)

TABLE 2

z(meters)	1	5	7	11
q	9.5	11.5	13.1	14.0
ϕ(rad)	0.1520	0.1841	0.2079	0.2240

The line fit in the higher NA launch case is not as good, indicating perhaps a deviation of the distribution from the

$$\phi^4 \propto z$$

dependence for modes very close to cut-off. The latter modes are excited in the NA = 0.4 launch case as the objective lens now matches the input NA of the fibre.

The use of the NA = 0.85 objective yielded no new information which is not unexpected as cladding modes were stripped from the fibre at launch.

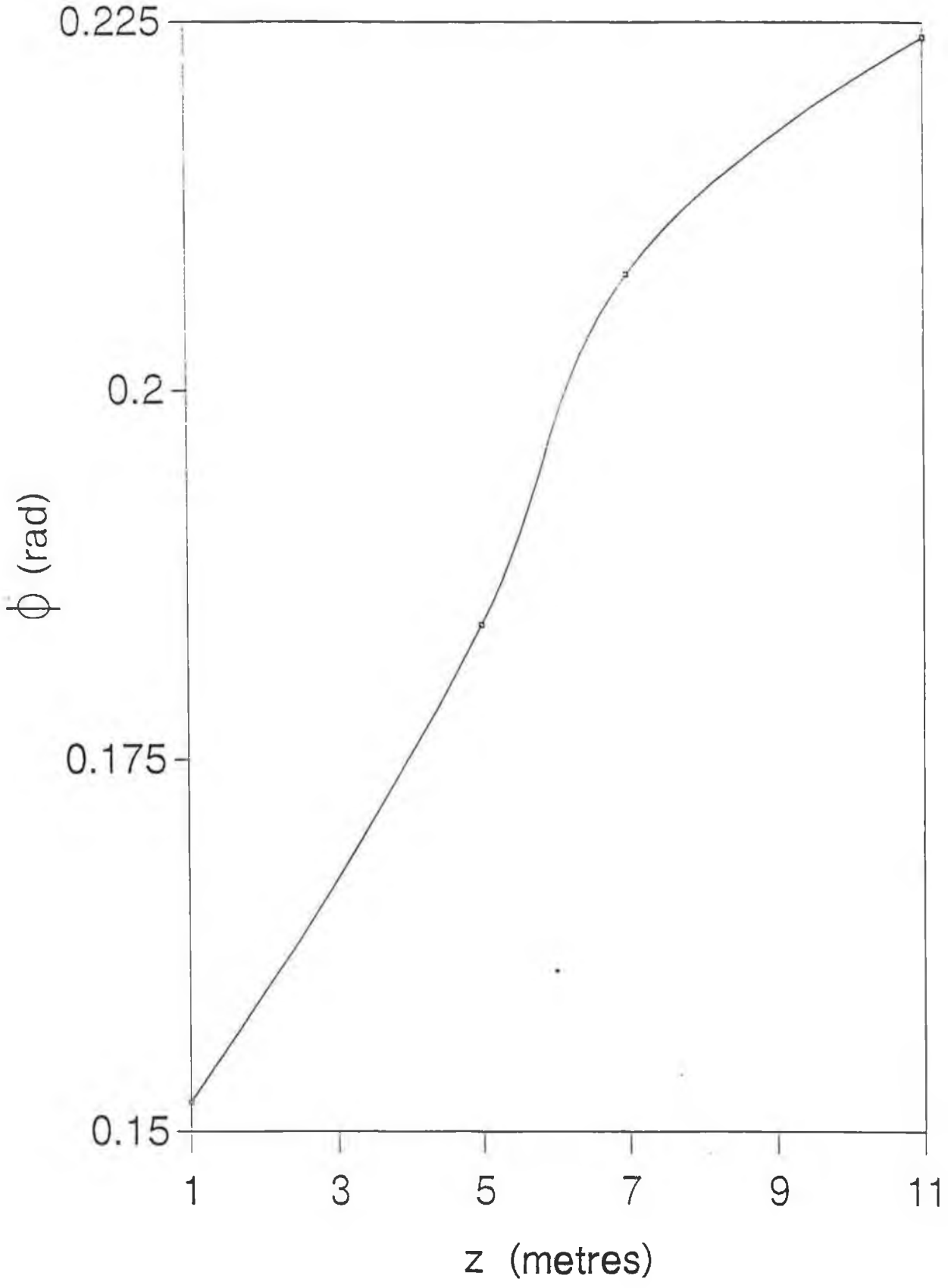

FIGURE 12: EXPERIMENTAL VARIATION OF Ø WITH z; NA = 0.4 LAUNCH OBJECTIVE.

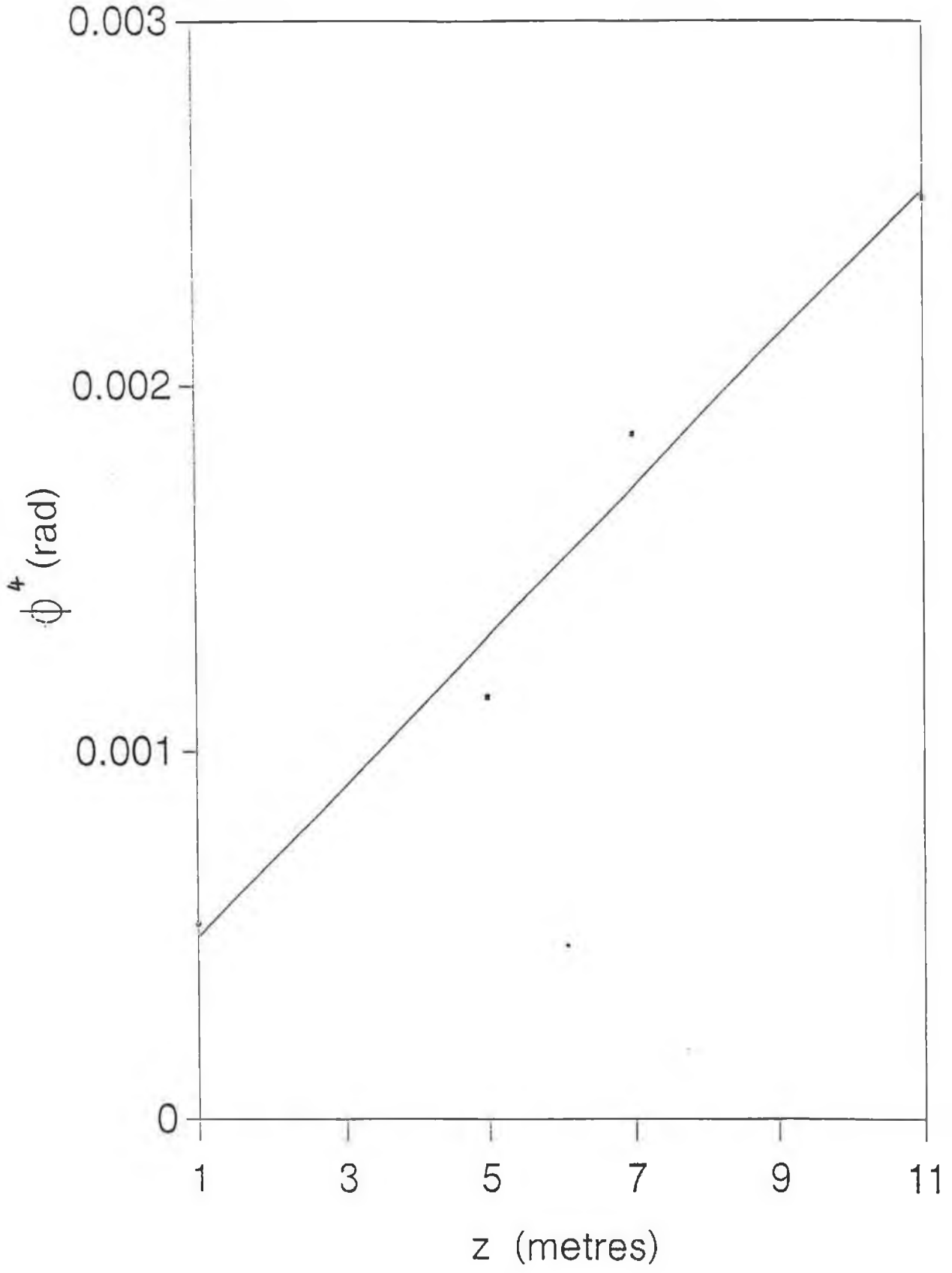

FIGURE 13: EXPERIMENTAL VARIATION OF ϕ^4 WITH z; NA = 0.4 LAUNCH OBJECTIVE.

4.3 MODE COUPLING THEORIES

In a multimode fibre the modes may be specified by two integers l and m. On a ray picture l is a measure of the extent of helical propagation, with large l values associated with modes that propagate in tightly spun helices. The parameter m is related to the angle θ that the ray makes with the fibre axis, as shown in fig 4.1.

For bound modes θ can have values in the range

$$0 \le \theta \le \theta_c \qquad with \quad \theta_c = \cos^{-1} n_2/n_1 \tag{4.3.1}$$

There are m field maxima along a radius vector and 2l maxima on a circumference. A mode characterised by particular values of l and m may be specified by a single integer M called the principal mode number given by

$$M = l + 2m \tag{4.3.2}$$

M has an upper bound given by the nearest integer value to $4V/\pi$, V being the fibre's normalised frequency. Each mode has a particular discrete value of the propagation constant ß given by

$$\beta = n_1 k Cos\theta \tag{4.3.3}$$

where $k = 2\pi/\lambda$ is the free space wavenumber of the light. ß is m fold degenerate ie for each value of ß there are m modes. ß is bounded between the values of n_1k and n_2k but the spacing between guided wave modes in ß space

$$n_2 k \le \beta \le n_1 k \tag{4.3.4}$$

decreases with decreasing mode number [Ref 13]

$$\Delta\beta \approx -\frac{\pi^2}{4n_1 k a^2} M \qquad 4.3.5$$

i.e as ß depends on θ (Eqn 4.3.3) this means that higher order modes are separated by larger angles than are lower order ones. Hence it is reasonable to expect that the interaction between modes would be strongest for lower order modes and weakest for higher order ones. In his original model of inter modal coupling Gloge [Ref 14] derived a power flow equation

$$\frac{\delta P(\theta,z)}{\delta z} = -\alpha(\theta)P(\theta,z) + (\Delta\theta)^2 \frac{1}{\theta}\frac{\delta}{\delta\theta}\left[\theta d(\theta)\frac{\delta P(\theta,z)}{\delta\theta}\right] \qquad 4.3.6$$

where $P(\theta,z)$ = optical power as a function of axial angle θ and distance z

$\Delta\theta = \lambda/4an_1$ = angular separation of propagation directions of neighbouring modes groups[1] ; a = core radius of fibre

λ = freespace wavelength

n_1 = core index

$d(\theta)$ = mode coupling coefficient (units of inverse length)

$\alpha(\theta)$ = attenuation coefficient as a function of θ.

The first term $\alpha(\theta)$ refers to mode attenuation as shown in Ref 4. If this is caused by evanescent wave absorption in the cladding then

---

[1]Footnote: For the work described here Δθ is of the order of one arc minute.

$$\alpha = A\theta^2 \qquad 4.3.7$$

to a good approximation [Ref 15] where

$$\textit{where} \qquad A = \frac{\alpha^*}{V\theta_c^2\sqrt{1-(\theta/\theta_c)^2}} \qquad 4.3.8$$

and α^* is the bulk attenuation coefficient of the cladding material at the wavelength λ.

For more accuracy replace θ and θ_c by $\sin\theta$ and $\sin\theta_c$ respectively.

The solution of Eqn 4.3.6 yields an equation for $P(\theta,z)$ which predicts how the modal power varies with θ as distance z is changed.

Solutions to this equation usually ignore the attenuation term in deriving $P(\theta,z)$ and correcting at the end by multiplying $P(\theta,z)$ by

$$\exp(-A\theta^2 z) \qquad 4.3.9$$

4.4 THE ANGLE INDEPENDENT COUPLING MODEL.

If - as originaly discussed - the mode coupling function $d(\theta)$is independent of θ then Eqn 4.3.6 has a solution which is a series of zero order Bessel functions [Ref 16] of the form,

$$P(\theta,Z)=\Sigma_n A_n \exp(-\beta_n^2 Z) J_0(\beta_n \frac{\theta}{\theta_c}) \qquad 4.4.1$$

where $Z = Dz/\theta_c^2$ and $D = d(\theta)(\Delta\theta)^2$.

β_n are roots of the zero order Bessel function.

$$J_0(\beta)=0 \qquad 4.4.2$$

and A_n are coefficients which depend upon the launching conditions.

When Z is sufficient large only the first term in the series is significant and $P(\theta,Z)$ reaches an equilibrium distribution of

$$J_0(\beta_1\theta/\theta_c)$$

This occurs for

$$\frac{Dz}{\theta_c^2} >> \frac{1}{25} \quad (approximately) \qquad 4.4.3$$

(25 being the approximate difference between β_2^2 and β_1^2).

In the functional form of Eqn 4.4.1 it is not clear how the width of the power distribution function $P(\theta,Z)$ varies with Z (ie with distance along the fibre).

To examine this a computer program was written to determine the full width at half power of P(θ,Z) as a function of Z for particular launch conditions.

The values of the coefficients A_n were determined from the launch conditions which were, for the purpose of the modelling, taken to be

$$P(\theta,0) = 1 \qquad for\ \theta_1 \le \theta \le \theta_2 \tag{4.4.4}$$

$$P(\theta,0) = 0\ for\ all\ other\ angles$$

θ_2 and θ_1 were taken to be 0.2 and 0.1 radians respectively (arbitrary values) and θ_c was taken to be 0.27 (the estimated value for the PCS fibre used). The boundary conditions (4.4.4) at launch give rise to the following

$$A_n = \frac{2\int_{\theta_1}^{\theta_2} \theta J_0(\beta_n \theta/\theta_c)\,d\theta}{\int_{\theta_1}^{\theta_2} \theta J_0^2(\beta_n \theta/\theta_c)\,d\theta} \tag{4.4.5}$$

$$= \frac{\frac{2}{\beta_n}\left[\left(\frac{\theta}{\theta_c}\right) J_1\left(\beta_n \frac{\theta}{\theta_c}\right)\right]_{\theta_1}^{\theta_2}}{\frac{1}{2}\left[\left(\frac{\theta}{\theta_c}\right)^2 J_0^2\left(\beta_n \frac{\theta}{\theta_c}\right)\right]_{\theta_1}^{\theta_2}}$$

using well known integral equations for zero order Bessel functions [Ref 17]. The series expansion of 4.4.1 is a Fourier - Bessel Expansion which generates a square wave in the limits $\theta_1 \le \theta \le \theta_2$ from an infinite series of zero order Bessel functions in an analogous fashion to a Fourier spectrum.

Using the equations listed in 4.4.5 a series of 56 values of A_n were generated by computer, using β_n values listed in Ref 18 for the first 20 and separations of π for the following 36 values. As can be seen in Fig 14 the coefficients A_n decrease slowly with increasing n and so many terms must be taken to express the square wave launch pulse as a series of Bessel functions. Fig 15 represents schematically the process being discussed. The program listed in Appendix 2 determined the FWHM values for a series of normalised distances Z ($=Dz/\theta_c^2$) for the fibre. The results are depicted in Fig 16. The pulse broadening as a function of normalised distance Z is seen to

(a) vary as $Z^{1/2}$ for $Z \leq 0.01$

(b) vary as $Z^{1/4}$ for $Z \geq 0.01$ 4.4.6

The latter result gives rise to the well known expression for the width of a pulse of light in a multimode fibre varying as $Z^{1/2}$ rather than Z as predicted by ray optics (pulse broadening in time is shown to depend on $\theta_{max}^2 z$ where θ_{max} is the largest value of θ. This is conventionally taken as the half power angular width ϕ. Due to diffusion θ_{max} is reduced from θ_c to a value which varies as $1/Z^{1/4}$ giving rise to a pulse broadening which scales as $Z^{1/2}$ rather than Z). As the experimentally observed broadening of ϕ/θ_c with Z scaled as $Z^{1/4}$ (see Figs 4.3 and 4.5) it would appear then this model of diffusion - with an angle independent coupling coefficient - is not valid. We will examine next a diffusion model in which

$$d(\theta) = d_0(\theta_c/\theta)^2 \qquad 4.3.16$$

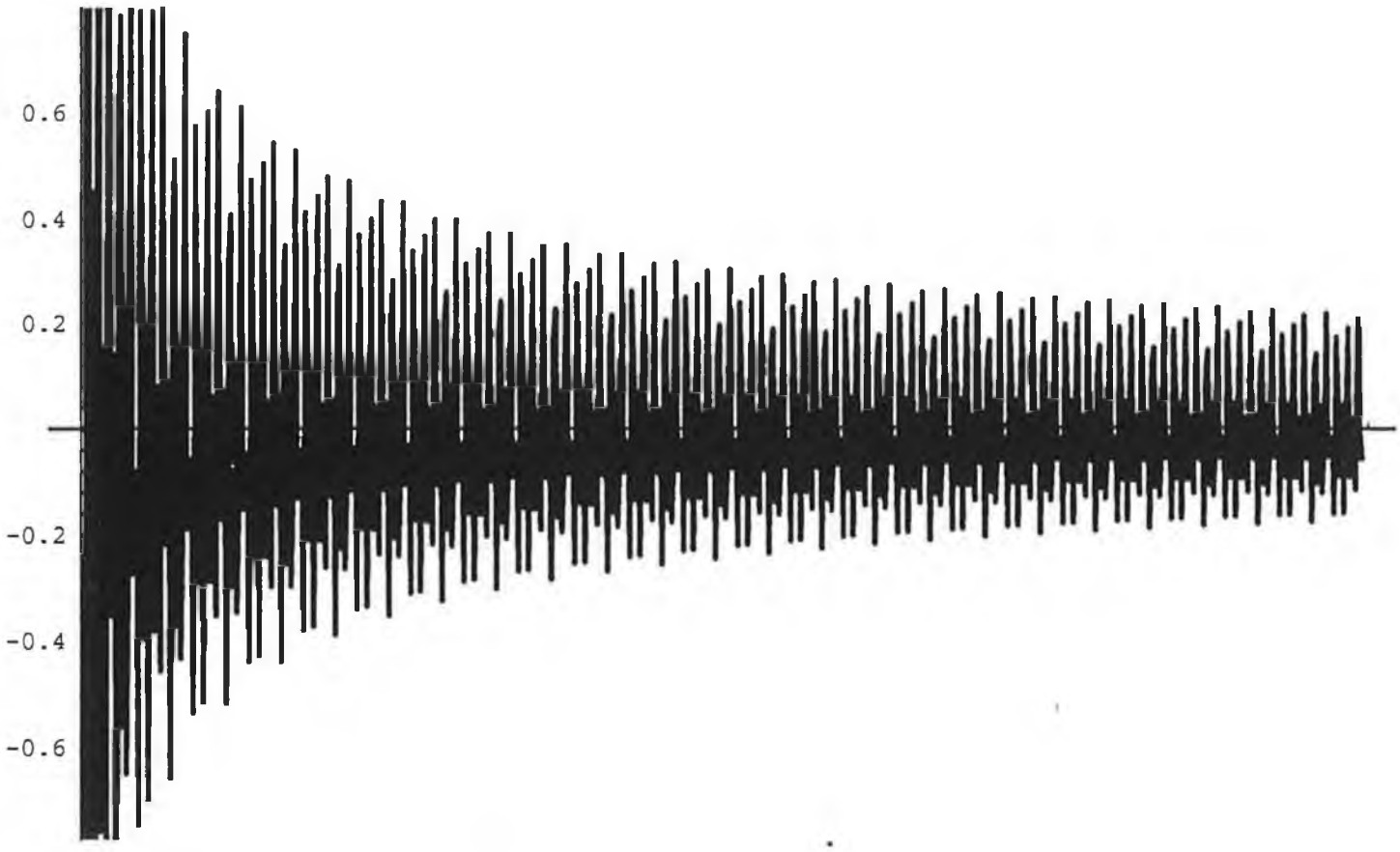

FIGURE 14: VALUES OF An VERSUS n FOR FOURIER-BESSEL EXPANSION.

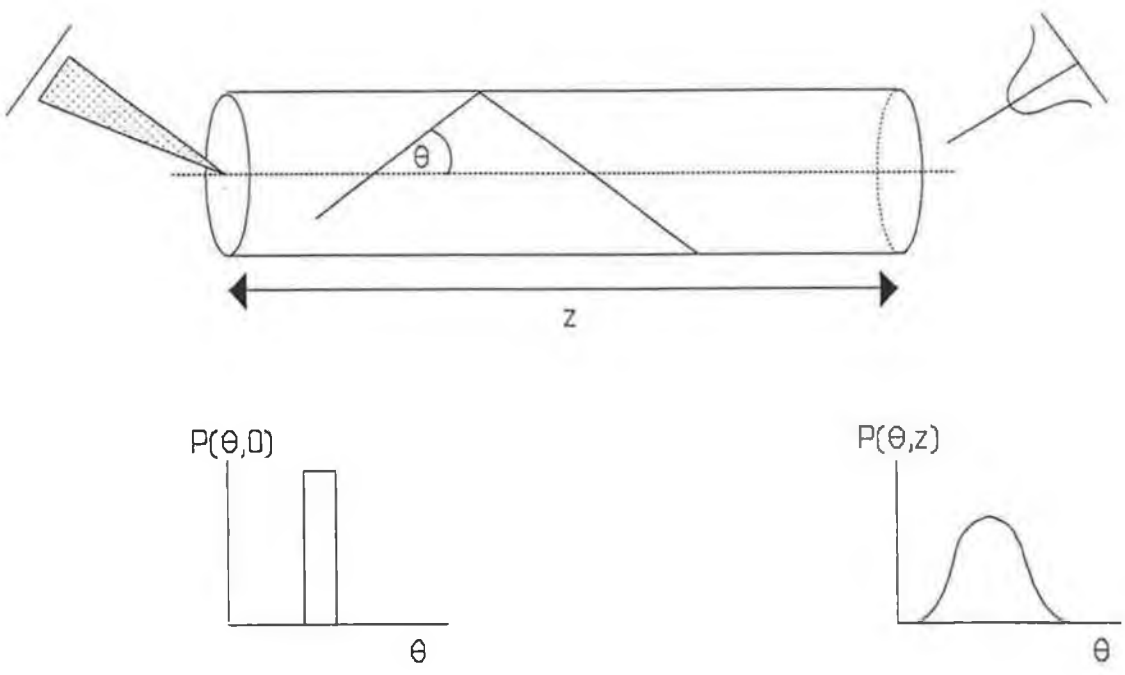

FIGURE 15: SCHEMATIC OF PULSE BROADENING DUE TO DIFFUSION.

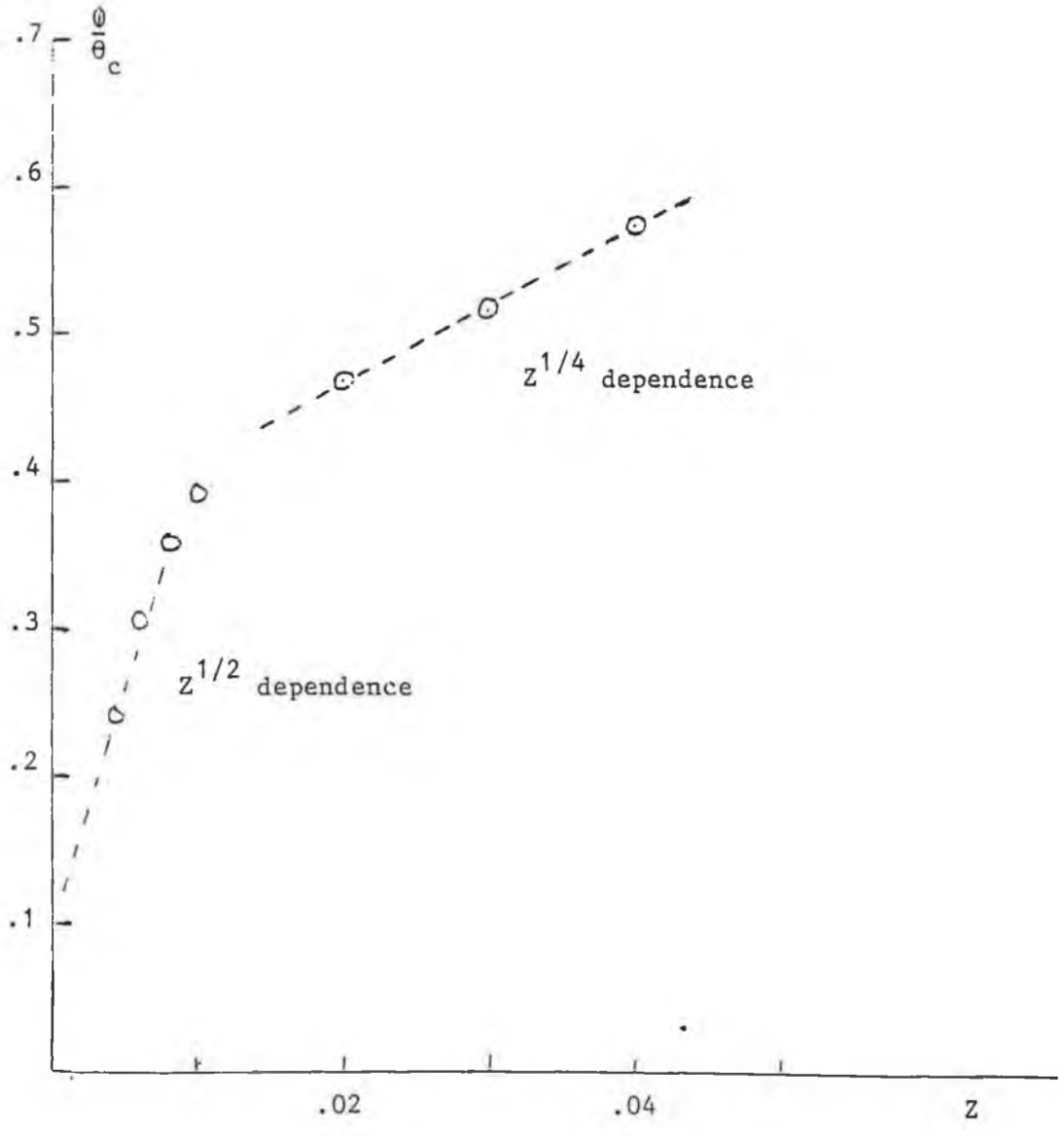

FIGURE 16: GLOGE MODEL, PULSE BROADENING AS A FUNCTION OF NORMALISED DISTANCE.

4.5 DIFFUSION WITH AN INVERSE θ^2 DEPENDENCE OF COUPLING COEFFICIENT.

Various groups have made measurements of the variation of the coupling coefficient in step index fibres with axial angle. As stated earlier in Section 4.3 mode coupling is expected to be strongest for low order modes. Olshansky and Oaks [Ref 19] found that the coupling coefficient followed an inverse power law dependence on principal mode number M. Marcuse et. al. [Ref 20] assumes a power coupling coefficient between neighbouring modes which scales as

$$\frac{1}{M^4} \qquad 4.5.1$$

or as $\mathrm{Sin}^{-2}\theta$ [Ref 21]. In the small angle (weakly guiding) approximation then the coupling coefficient follows a

$$\frac{1}{\theta^2} \qquad 4.5.2$$

dependence and following Herskowitz et. al. [Ref 22] we can write

$$d(\theta)=d_0(\theta_c/\theta)^2$$

and

$$D=d_0(\Delta\theta)^2 \qquad 4.5.3$$

Inserting the angle dependent coupling term in the expansion 4.4.1 as

$$\exp[-\beta_n^2 \frac{Dz}{\theta_c^2}(\frac{\theta_c}{\theta})^2] \qquad 4.5.4$$

we have investigated how the full width at half maximum varies with the normalised distance Z as before. [The same launch conditions as described in 4.4.4 and same values for θ_1 and θ_2 are taken]. The model data is shown in Fig 17. As can be seen

$$\phi/\theta_c \textit{ varies linearly with } Z^{1/4} \textit{ for } \theta<Z\leq 0.01 \qquad 4.5.5$$

The progressive widening of the initial "square wave pulse" with fibre length is seen in Fig 18. Each curve is normalised with respect to the maximum value of P(θ). The slope of the linear region is estimated to be 2.70. Herskowitz et. al. [Ref 22] model the propagation of a power distribution of the form

$$P(\theta,z) = f(z)\exp(-\theta^4/\phi^4)$$

and find that

$$(\frac{\phi}{\theta_c})^4 = 16\frac{Dz}{\theta_c^2} + (\frac{\phi_0}{\theta_c}) = 16Z + \phi_0/\theta_c \qquad 4.5.6$$

i.e that the slope of the

$$(\phi/\theta_c) \text{ versus } Z^{1/4}$$

graph is 2.0. Their launch pulse being exponential never reaches zero unlike the square wave launch pulse used in our model.

Fig 18 shows graphically how the model predicts the power distribution function P(θ,z)for various values of Z in (0.0,0.01).

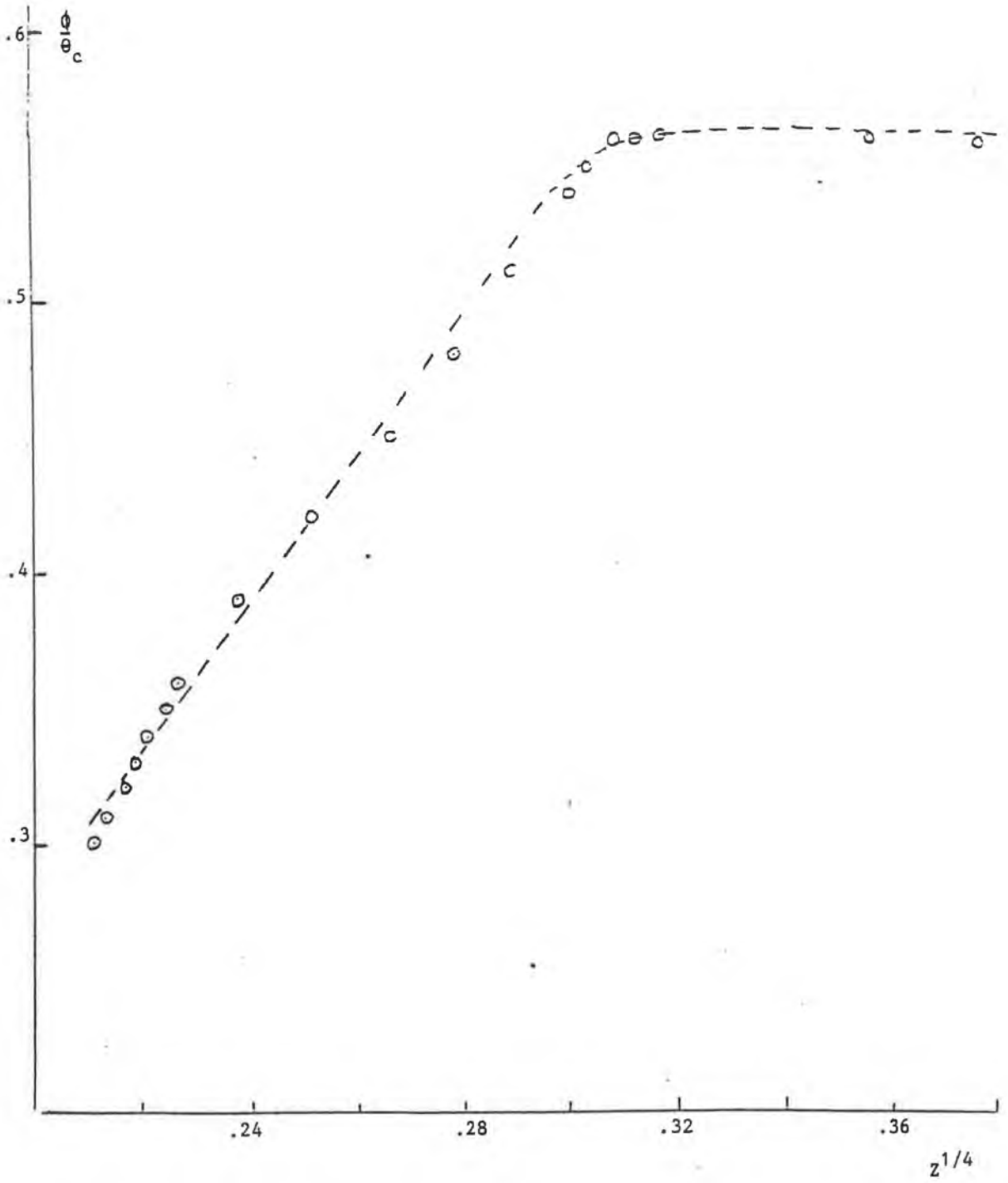

FIGURE 17: ANGLE DEPENDENT COUPLING MODEL.
VARIATION OF ϕ WITH LENGTH.

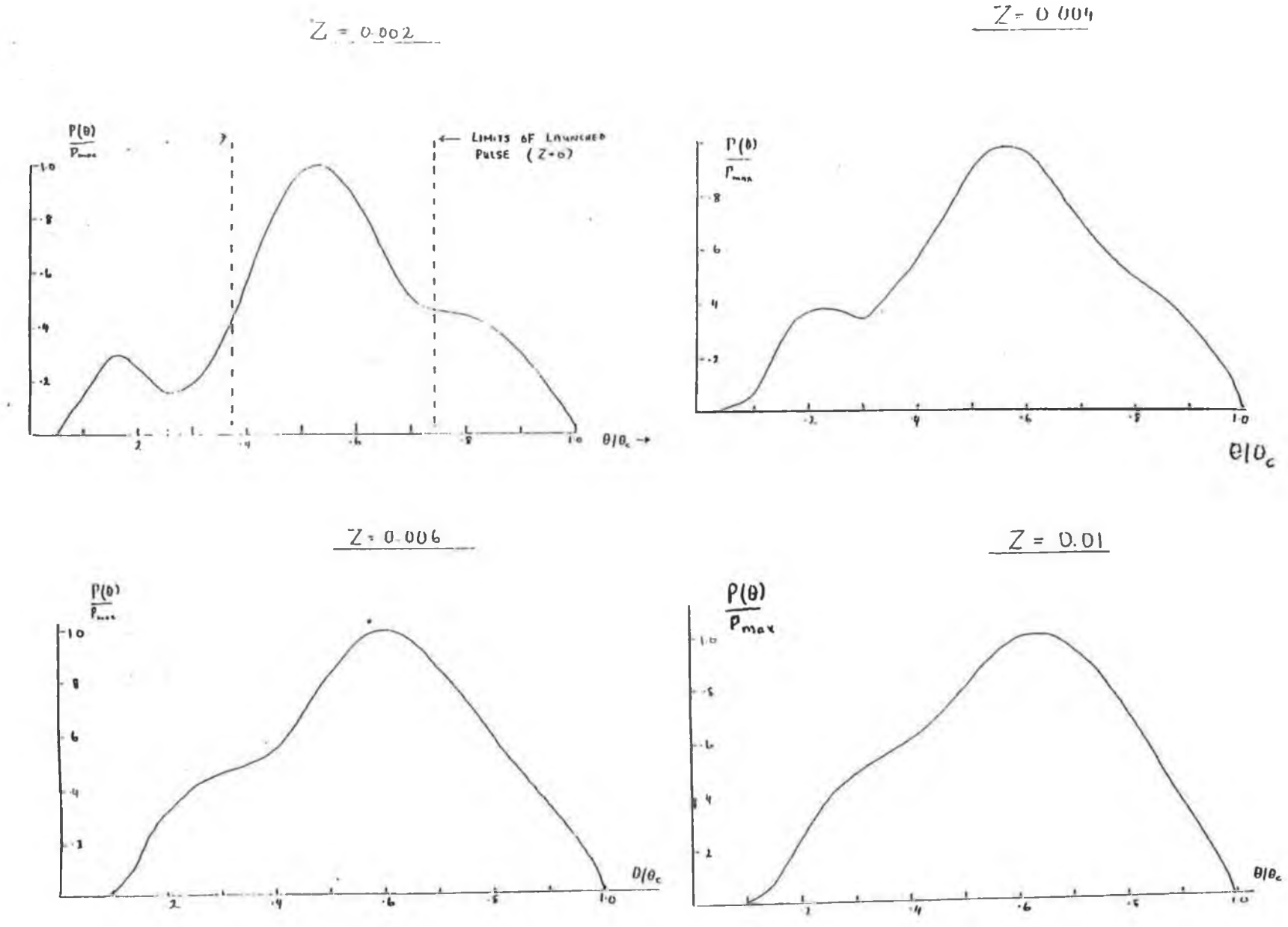

FIGURE 18: BROADENING OF SQUARE WAVE PULSE WITH DISTANCE, ALL CURVES ARE NORMALISED W.R.T. Pmax.

The $1/\theta^2$ dependence of the mode coupling coefficient has been attributed by Olshansky [Ref 19] to microbending or random curvature of the waveguide axis.

Assuming a graph slope of 2.70 the diffusion coefficient D for the fibre used is calculated to be

$D = 1.17 \times 10^{-5}$ rad^2/m using Fig 4.3

$D = 1.02 \times 10^{-5}$ rad^2/m using Fig 4.5

4.6 COMPARISON WITH OTHER MEASUREMENTS

Not many values for modal coupling coefficients are available in the literature. Herskowitz et. al. [Ref 22] made a series of measurements on silica fibre (ITT No 011289 and ITT No. 012579.B) for which core and cladding material was silica and quoted values of

$D = 1.2 \times 10^{-7}$ rad^2/m

$D = 2.5 \times 10^{-7}$ rad^2/m

for the 80 μm core fibre. This is a factor of about two orders of magnitude lower than our measurement. It would appear therefore that the existence of polymer cladding increases the coupling between modes in a silica core fibre. More recently Dugas and Maurer [Ref 23] measured values of

0.38 rad^2/m

0.96 rad^2/m

for all plastic fibres (i.e. core and cladding materials are both polymers.

They attribute the high coupling coefficients to longitudional microcracks of the PMMA[2] caused by stress relaxation during fibre drawing. No D values for plastic clad silica fibre such as used here have been found in the literature.

4.7 SIGNIFICANCE OF MODE COUPLING TO EVANESCENT WAVE SENSING

As shown in Chapter 1 the attenuation coefficient for evanescent wave spectroscopy depends on the penetration depth of the evanescent wave into the chemical and as a result depends strongly on the fraction of the optical power that exists as higher order modes in the sensing region. If the power is transmitted to the sensing area by a long length of fibre then intermodal coupling will have reduced the power in higher order modes and accordingly reduced the sensitivity of the absorption technique. Likewise any narrowing of a launched pulse due to absorption of higher order modes in the sensing region will be counteracted by broadening due to intermodal coupling. Thus significant amounts of mode coupling mitigate against detection sensitivity in evanescent wave fibre sensors where the lead in fibre (source-to-sensor) has a length greater than above

$$\frac{0.01\ \theta_c^2}{D} \approx 4x10^{-3}\ \frac{(NA)^2}{D} \qquad 4.6.1$$

for silica core fibres (n = 1.5) of numerical apeture NA. Taking a value of D of

---

[2]Footnote: Polymethyl Methacrylate.

approx

1×10^{-5} rad^2/m for PCS-600 fibre and NA = 0.4

this gives a maximum lead-in length of about

70 m

For much shorter lead-in lengths than this a high order mode pattern impressed at the source end will be effectively maintained at the sensing region. For much larger lead-in lengths the mode equilibrium will have set in and the power distribution will have stabilised to a

$$J_0(\beta\frac{\theta}{\theta_c}) \qquad 4.6.2$$

distribution. In this case the power attenuation coefficients (γ) due to evanescent wave absorption in the sensing region which are given in Ref 4 for unclad fibre sensing and in Ref. 12 for porous clad fibre sensing can be modified by including the power distribution function 4.6.2 in the integrals. Using the modified expressions for γ then an experimentally measured power attenuation can be used to extract a species concentration (where the absorptivity is known).

If the sensing region is located a substantial distance from the detector (as for example in the case of an Optical Time Domain Reflectometer measurement of attenuation) then intermode coupling will tend to broaden the returned optical pulse which has been narrowed by evanescent wave absoption in the sensing region.

4.8 CONCLUSION.

Intermodal coupling in PCS-600 fibre is significant over distances of the order of 70m. Such coupling reduces substantially the detection sensitivity of chemical species present in the cladding region of such fibres where the sensing zone is located more that typically 50m from the optical source for such fibres.

At the time of preparing this document similar work was reported by Norris and Smith [Ref 24]. Using a linear diode array (Oriel Instaspec) with 512 elements and a broadband LED source they investigated modal coupling in eight step index fibres, one of which was the Quartz et Silice PCS 600 fibre used in this work. They observed "possibility linear broadening with length for on axis modes but little change for off axis modes" They concluded that " at a length of 50 m the modal preservation was excellent and so any changes with length would have been very small, too small to detect in this experiment". It would appear then that our two dimensional detector array approach offers greater detection sensitivity for modal coupling measurements on large diameter step index fibres. This is not surprising as the 2-D camera system records much more optical power data than the linear array.

REFERENCES (CHAPTER 4):

13. Marcuse D. "Theory of Dielectric Optical Waveguides" (Academic Press NY 1974) Eqn 5.5-86 p 217

14. D. Gloge "Optical Power Flow In Multimode Fibres" Bell. Syst. Tech. J. 51 p 1767 (1972)

15. Synder A. and Love J.D. "Optical Waveguide Theory" (Chapman & Hall 1983) Eqn 6-21 p 127.

16. Rousseau M. and Jeunhomme L. " Numerical Solution Of The Coupled Power Equation In Step Index Optical Fibres" I.E.E.E. Trans Microwave Theory Tech. MTT-25 p 577 (1977)

17. O'Neill P. " Advanced Engineering Mathematics" (Wadsworth Publ. Co. 1983) p 814, 815

18. Abramowitz M. and Stegun I.A. "Handbook of Mathematical Functions" (Nat. Bur. Standards 1964) Table 9.5 p 409

19. Olshansky R. and Oaks S.M. Appl. Optics 17 11 p 1830 (1978)

20. Marcuse D, Gloge D, Marcatili E.A. " Optical Fibre Telecommunications" (Academic Press N.Y. 1979 eds. S.E. Miller, A.G. Chynoweth) Ch. 3. Section 3.11 p 89.

21. Cheo Pk "Fibre Optics And Oploelectronics" (Prentice Hall Int. 1990) Eqn 4.133 p 71.

22. Herskowitz G, Kobrinski H and Levy. U. J.L.W.T. LT-1 p 548 (1983)

23. Dugas J. and Maurel G. " Mode - Coupling processes in Polymethyl methacrylate - core optical fibres" Appl. Opt. 31 (24) 5069, (1992)

24. Norris, J.O.W. and Smith A.P. "Experimental quantification of intermodal conversion in multimode optical fibres" prepared for Optical Sensors Collaborative Association Documents No 92/11 F.

APPENDIX 1

The I-SCAN Linear Array System.

This Appendix describes the design, construction and testing of electronics used to display in hard copy form (i.e. suitable for a chart recorder) a one dimensional optical image created by a 256 element linear CCD 111 chip. The operation of a CCD array is described and the unit which was constructed to download images is discussed in detail.

CCD THEORY

A Charge-Coupled Device is a semiconductor in which finite isolated charge packets are transported from one position in a semiconductor to an adjacent position by sequential clocking of an array of gates. The charge packets are minority carriers with respect to the semiconductor substrate.

The CCD can store and transfer analog charge signals, either electrons or holes, that may be introduced electrically or optically. The CCD operates by storage and transfer of charge, representing information, between potential wells at, or near the surface of silicon. The potential wells are formed by closely spaced MOS Capacitors that are being pulsed into deep depletion mode by a multiphase clock voltage. The charge is moved about the surface by moving the potential minima using appropriate voltages applied to the conductors of the MOS capacitors. The CCD is a dynamic device in which charge can only be stored for times much shorter than the thermal relaxation time for its MOS capacitors.

THE MOS CAPACITOR

CCDs were first discovered in 1969 but their concept is based on the MOS capacitor. A MOS capacitor differs from an ordinary capacitor in that the bottom metal plate is removed and replaced with a semiconductor.

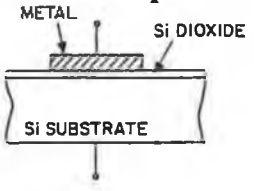

Fig. 1. Cross sectional view of an MOS Capacitor.

Suppose we use p-type silicon in the substrate, doped with acceptor impurities (free holes). Appling a negative DC voltage and the holes will accumulate at the Si/SiO_2 interface.

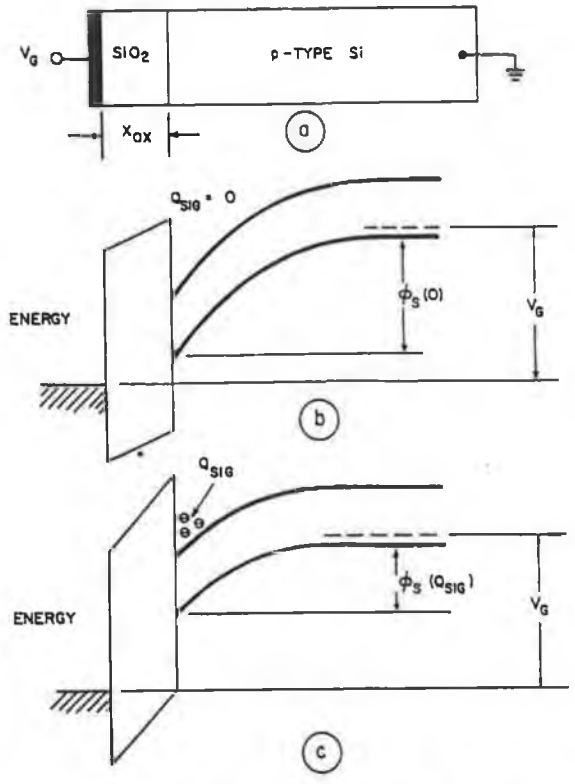

Fig. 2. Band structure for an MOS capacitor.

When a voltage is applied to the conducting electrode of an MOS capacitor the energy bands bend. Fig. 2b above shows the energy bands at the semiconductor/insulator interface with the field applied in a direction to repel minority carriers. A potential well of depth ϕs_0 is formed at the interface under the electrode. Fig. 2c above shows the situation at a later stage when the potential well has been partially filled to ϕs due to photon absorption, injection from an input diffusion or thermal generation.

SURFACE vs BURIED CHANNEL CCDs

A CCD can be constructed either as a surface channel device or as a buried channel device. The potential wells for the SCCD is formed at the Si/SiO_2 interface while the BCCD forms wells below the surface to avoid charge trapping by surface states. BCCDs have higher frequency response than SCCDs with the same dimensions. The maximum charge signal in a BCCD is up to three times smaller than that of a SCCD.

CHARGE TRANSFER ACTION

The application of a positive voltage V_1 to the gate electrode forms a depletion region in the p-type silicon below the gate, thus forming a potential well at the Si/SiO_2 interface. In a three phase clocking system charge can be transferred to the next, and deeper potential well at $V_2 > V_1$, and then to $V_3 > V_2$ etc... The direction of charge flow is determined by the clock phase sequence.

Charge is transferred in the three phase system shown in Fig.3 as follows: In Fig. 3a $V_2 > V_1$ so the potential well beneath the electrode connected to this line is deeper than under electrodes 2 and 3. The photogenerated minority carriers will collect under electrode 1. Next electrode 2 is made more positive than electrode 1 leaving 3 in its initial state. Fig. 3b shows the potential wells beneath the electrodes. Electrons can now tunnel from one well to the next. Finally the charge can be left under electrode 2 as shown in Fig. 3c. By continued application of these voltages, photogenerated minority charge can be moved through the structure.

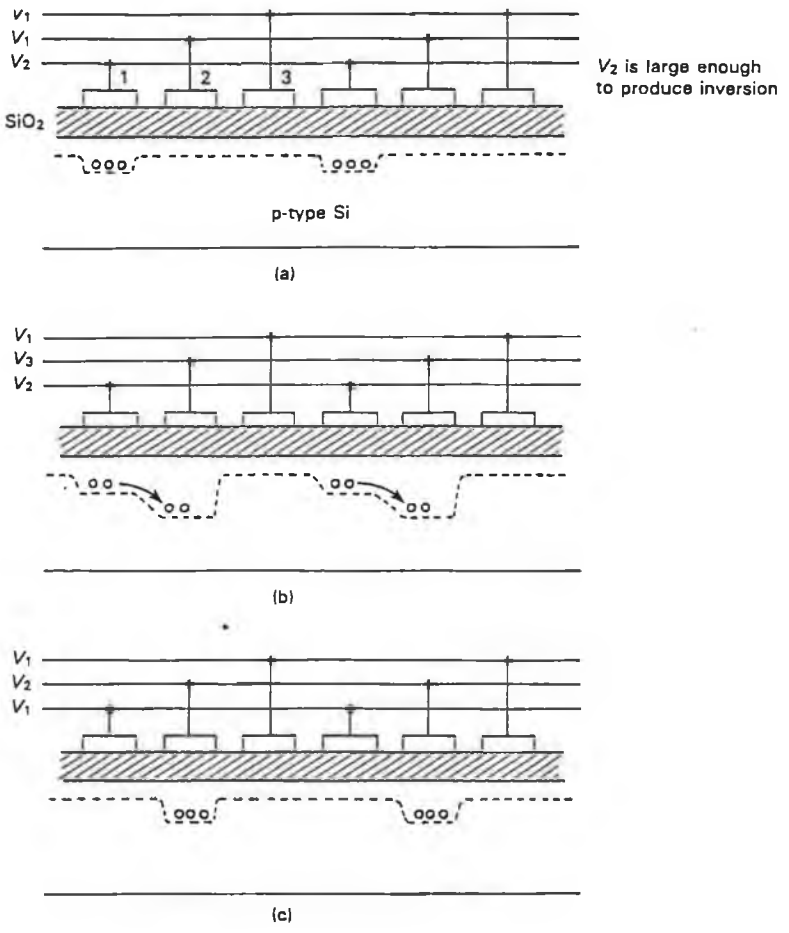

Fig. 3. Charge transfer action in a three phase system.

There is no significant charge build up in a particular well because charges are being continually swept out. The three phase system described above is symmetrical and the direction of charge flow is determined by the clock phase sequence. Operation of systems with less than three phase clocks require an asymmetry in the CCD structure to determine the direction of flow.

In a two phase system such as that in the Fairchild CCD111, there is a need to produce a directionality in the structure. One example of how to do this

is to produce an ion implanted layer under alternate electrodes. On application of a voltage to two electrodes, the potential barrier under the electrode containing the layer is smaller than that under the other electrode, thus direction can be added to the structure.

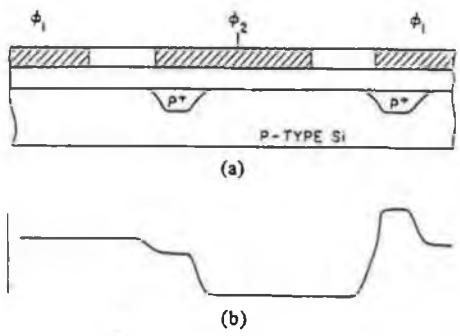

Fig. 4. Implanted barrier two phase CCD.

Fig. 4a above shows a cross sectional view of the structure while Fig. 4b displays the surface potential profile showing built in potential barriers due to non uniform doping.

LINE IMAGERS

In this mode clocks are stopped for an appropriate integration period while the information is clocked out of the device. A potential disadvantage is that light still falls on the device while the information is being clocked out, but some type of mirror or mechanical shutter assembly could be used to avoid this. Alternatively, a solution used in most commercial devices is a special imaging register combined with a transfer electrode system whereby the image signal may be transferred into a CCD readout register which is itself shielded from light.

Line imagers require that all imaging sites are in a straight line, that signals can be read out of the imaging registers to one or more transfer registers used to convey the signal to the output. They must also minimise the number of outputs for best overall transfer efficiency and minimise the length and width of the device for physical fabrication and packaging. In a twin readout structure, each alternate photogate is switched to an alternate register.

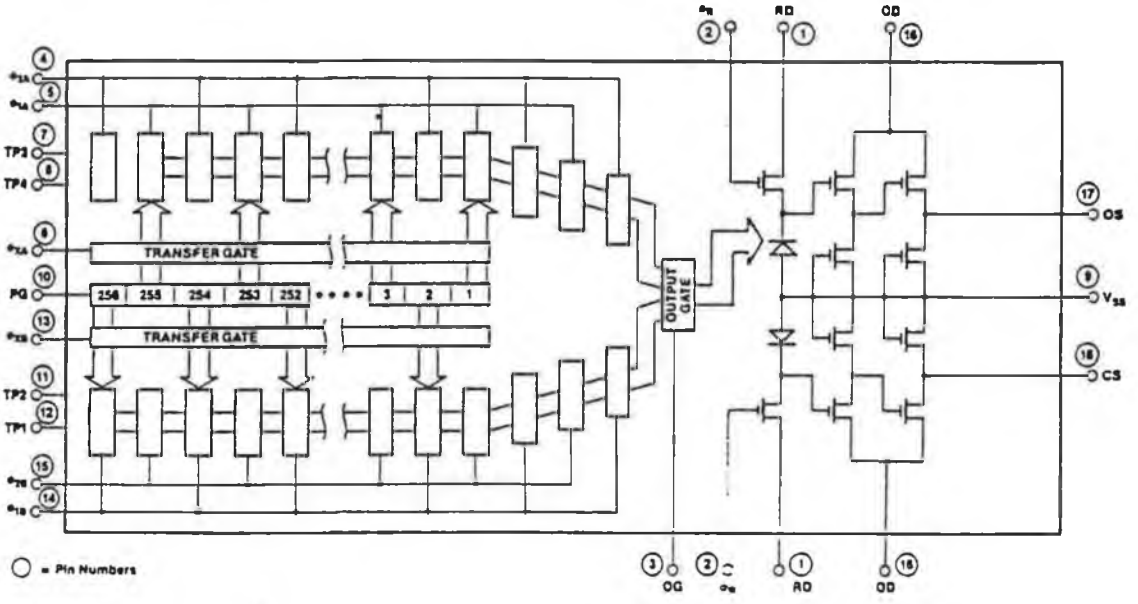

Fig. 5. Circuit diagram of a Fairchild CCD 111.

Reproduced from CCD 111 Specification.

NOISE IN CCDs

CCDs are inherently low noise devices in that packets of minority carriers are kept isolated inside the semiconductor during the storage/transfer process. Some forms of noise which effect the device are:

1) SHOT NOISE - The number of electrons in a charge packet has an uncertainty. This uncertainty becomes noise for the charge packet.

2) TRAPPING NOISE - The charge trapping and emission process by the surface states and bulk traps include noise to the signal charge packets since the trapping and emission processes are random. For surface channel CCDs the surface states are the dominant noise source while for buried channel devices, bulk trapping represents the major noise source.

3) kTC NOISE - Charge detection methods normally involve the charging of a capacitor to some level. When a capacitor is charged through a resistor the voltage across the capacitor contains some noise due to the voltage fluctuations across the resistor.

4) DARK CURRENT - Consider a CCD operating without any charge packet, either electrically or optically. All MOS capacitors made up with electrodes are then in deep depletion and thermally generated carriers will be collected in the energy wells. This dark current flows in a device operating in complete darkness.

THE FAIRCHILD CCD 111.

The Fairchild CCD 111 is a monolithic 256 element line image sensor designed for optical character recognition and other imaging applications that require high sensitivity and speed. The sensor is manufactured using CCD n-channel isoplanar buried channel technology and the chip includes 256 pixels, 2 charge transfer gates, two 2-phase analog transport shift registers, an output charge amplifier and a compensation amplifier.

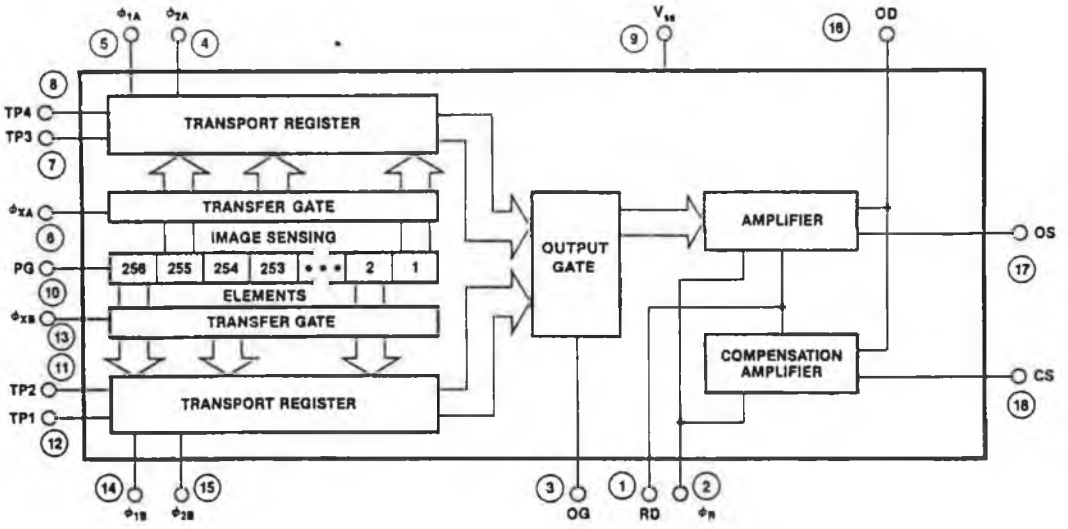

Fig. 6. Block Diagram of the CCD 111

Reproduced from CCD 111 Specification.

Operation of the device is as follows: Image photons pass through the transparent polycrystalline silicon photogate and are accumulated in the photosites. The charge packets are then transferred out of the image sensors to the transport registers via the transfer gates. The odd numbered pixels have their

charge transferred to one transport register while the even numbered pixels have their charge transferred to the other. ϕx_A and ϕx_B are the transfer clocks used to clock the information from the pixels to the transport registers, while $\phi 1_A$,$\phi 1_B$, $\phi 2_A$ and $\phi 2_B$ are two sets of two phase waveforms used to move the image information from the transport registers to the amplifier, whose potential changes linearly in response to the quantity of signal charge delivered.

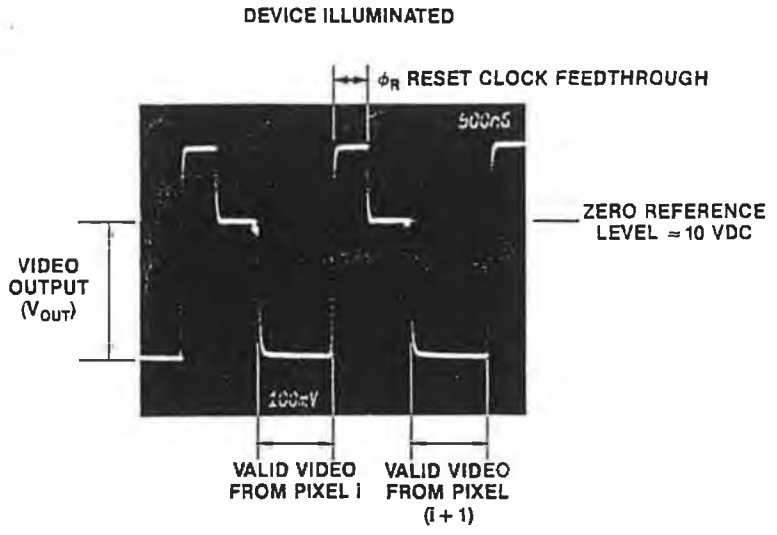

Fig. 7. Output of two pixels.

Reproduced from CCD 111 Specification.

Above is a picture of the output of two pixels as seen on an oscilloscope screen. Note that the valid video signal from pixel i is only a portion of the output for that particular pixel. The rest of the output is made up from the reset clock feedthrough and a zero reference level - the signal from a pixel in the dark.

In this operation we are using a design development board called an

I-SCAN, which comes fully assembled and requires only power and an oscilloscope to display the video information corresponding to the light incident on the sensor. There is an internal / external master clock select signal which determines if the master clock will be generated on the board or input from a function generator or other source. There is also an internal / external exposure sync signal which determines if the "start of scan" signal is generated on the board or externally, thus the data rate of the CCD and the time between scans can be adjusted externally by use of function generators or other signal sources.

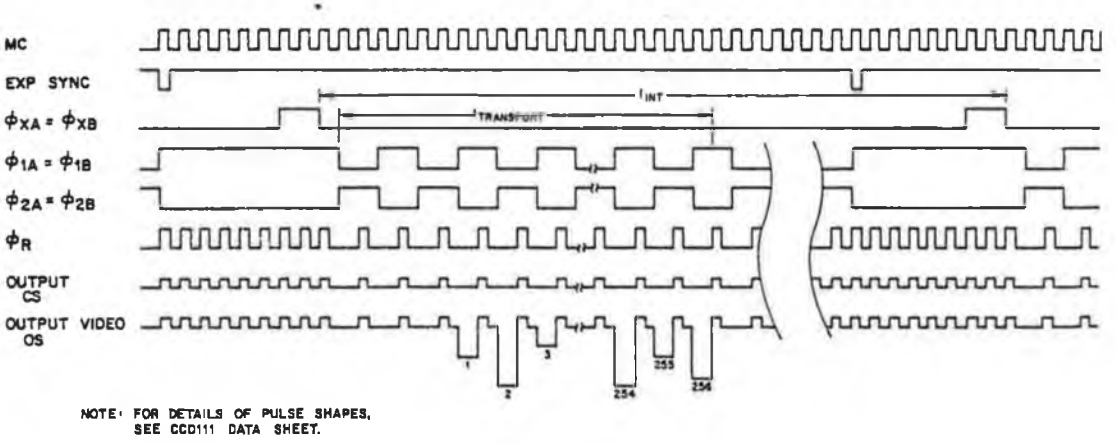

Fig. 8. I-SCAN timing diagram.

Reproduced from CCD 111 Specification.

Note that the video output is at half the frequency of the master clock signal. The master clock is divided by two immediately on entering the board and all processing done at this lower frequency. See I-SCAN Specification, Attachment 1.

We require hard copies of the information scanned by the sensor. However, the internal clocks only give the output data rate in the range 1 to 10MHz and although the image on the oscilloscope screen represents the light incident on the array, this is too fast for output to a chart recorder. A data rate of about 10Hz is needed for a chart recorder output. In order to slow down the output signal from the I-SCAN card an external frequency source was used. It was found that at frequencies in the range of 100 - 150KHz the output was clear, but at lower frequencies the data becomes very susceptible to noise. Altering the width of the crests and troughs of the input square wave just changed the width of the timing reference and voltage reference signals.

Some method of slowing down this 100KHz signal to a frequency in the chart recorder range needed to be found. A/D conversion and writing to a RAM, then reading to the D/A port of a computer or using a Fairchild CCD321B-3 Time Base Compression delay line was considered, but a more effective route was considered to be the preparation of a Sample-and-Hold circuit to select that part of the signal that represented the intensity information and feed it to a chart recorder at 10 Hz.

THE SAMPLE-AND-HOLD CIRCUIT

The sample-and-hold circuit used for processing the video signal operates as follows; The video signal is fed through a buffer amplifier, (for protection of the sample-and-hold), into the sample-and-hold amplifier and it is sampled at certain intervals. The output of the sample-and-hold was fed through a buffer to the chart recorder. The critical factor is the trigger signal for the sample-and-hold amplifier.

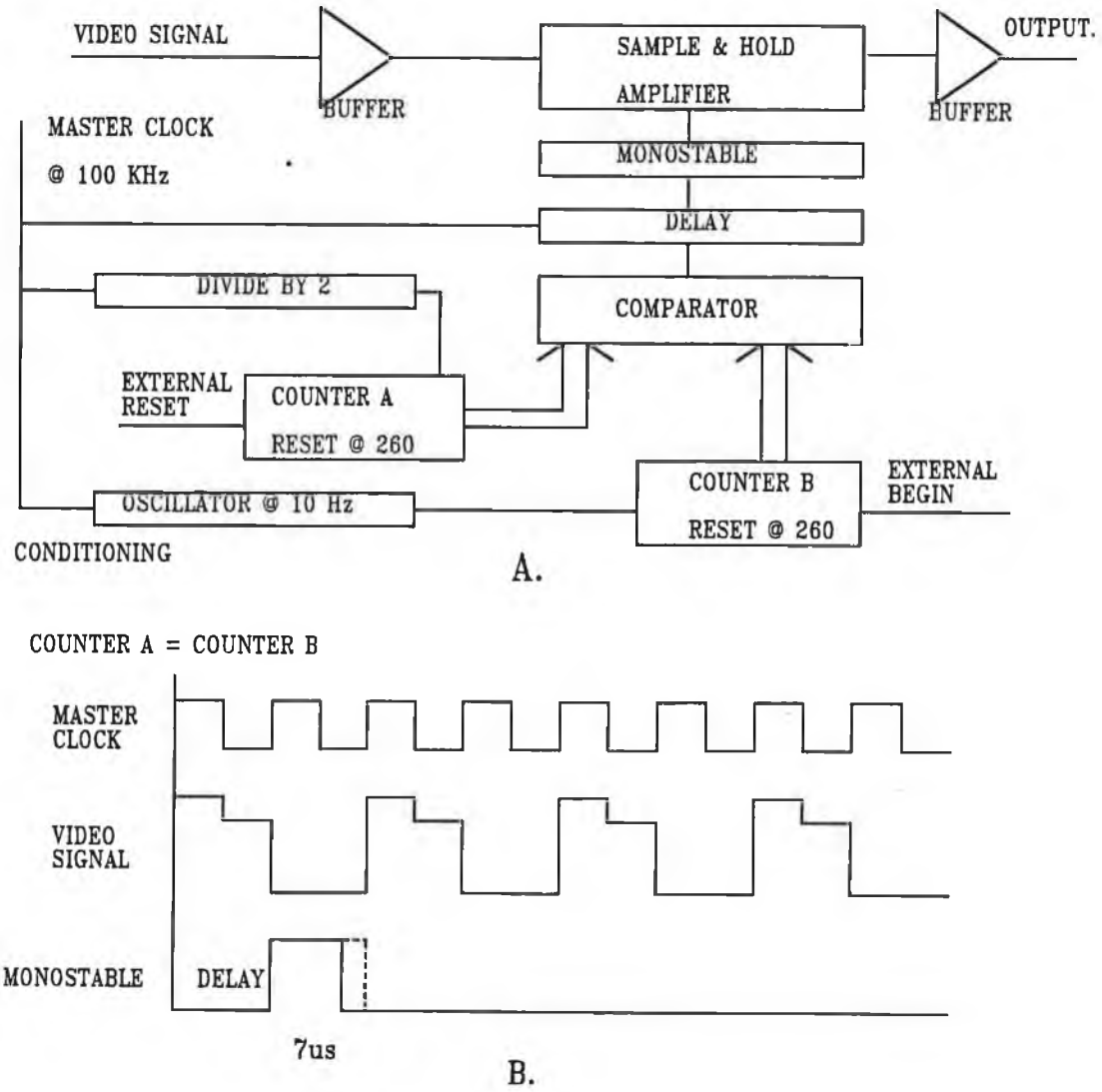

FIG. 9. Block diagram of the Sample-and-Hold circuit and its timing diagram.

The master clock for this circuit is at the same frequency as that for the I-SCAN. This master clock comes onto the board, from the same source as that used for the I-SCAN, and the frequency is halved since the data rate is half the clock speed on the master board. This signal is now at the same frequency as the data rate from the I-SCAN board. The clock signal is now fed through a counter which is configured to reset at a count of 260. The reason for choosing 260 is that there are two blank pixels at the beginning and end of each scan. The reset is achieved by bits 3 and 9 of the counter being ANDed and the result fed to the counter reset pin. This counter should have an "external begin" input.

Meanwhile an oscillator is operating at 10Hz producing a square wave that is synchronised with the fast clock using a D Type flip flop. The slow clock is also fed to a counter which is configured to reset at 260. This counter has an external reset also. The outputs of both these counters are fed into a comparator. Both counters are counting from 1 to 260, one fast and one slow. When these counts are equal, i.e. when both counters read pixel i, the comparator output is latched high. The comparator output is delayed for one clock cycle, (see timing diagram, Fig. 9b), and then a monostable is latched on. The monostable timing is dependant on its RC circuit, in this case 7μs. This complete process happens for i = 1 to 260, and then, depending on the reset configuration, it either begins again or else waits for another "begin scan" pulse.

SYNCHRONISATION

Some sort of control is required over the slow clock so that the system can be set to run every time a scan is required and it will stop when the scan is complete. A SR flip flop works on the basis that S and R are normally high and Q is low. If R is set low then Q goes high and remains so until S is pulsed low. Then Q goes and stays low. The reset configuration for the slow clock is as follows.

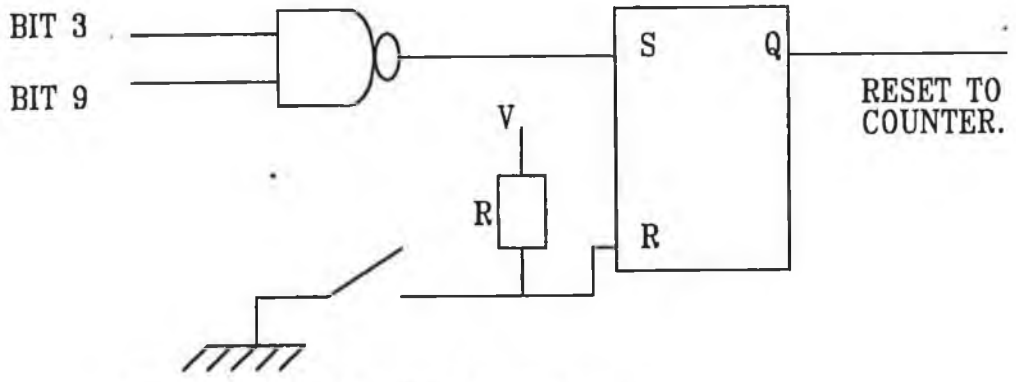

Fig. 10. Reset for the slow clock.

The next problem was to synchronise the fast clock with the clock on the I-SCAN board so that the fast clock starts when the scan starts, counts to 260 in sync with the CCD data output and when completed stops and waits until the I-SCAN is about to take another scan.

Pin 15 of the I-SCAN board provides a clock signal which is at half the frequency from the function generator. Using this as the S/H circuit fast clock, instead of using a D Type flip flop to divide the external master clock by two, will improve the synchronisation. The other D Type flip flop is still used to condition the slow clock. The only difference from before is that the fast clock now comes

directly from the I-SCAN board to the flip flop and on to the counter.

The next step is to have the scan and fast count begin and end together. There is an Exposure Sync signal which pulses at the beginning of every scan. It was considered that this signal be used to set the fast clocks running using another SR flip flop latch as follows:

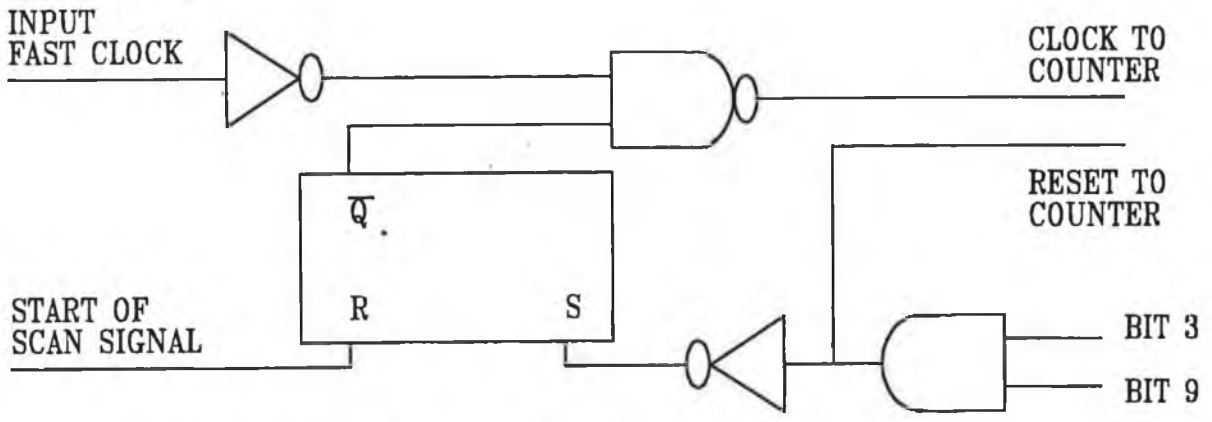

Fig. 11. Reset for the fast clock.

In this system the clock is fed into the counter via a dual input NAND gate, the other input being from the $\bar{Q}$ output of the SR flip flop. The flip flop is configured to set at a count of 260, thus stopping the clocks. At this stage the counter will also be reset. The flip flop will be reset again, (restarting the clocks), by a signal that indicates start of scan.

Pin 14 of the I-SCAN board is the Exposure Sync signal. This is normally high but pulses low at the start of every scan. The possibility of using this signal for start of scan and hence start of fast pulse was considered. On examining this signal on the oscilloscope it was found that, as in the I-SCAN timing spec, the

exposure sync signal preceedes eight clock pulses and then the video signal from the pixels. The Exposure Sync pulse, (see diagram 12), is generated by two monostable latches and is fed to pin 1, (memory reset), of counter U5, 74LS161PC. The purpose of this counter is to control the transfer pulse through driver U7 and to stop the transport clocks during the transfer pulse.

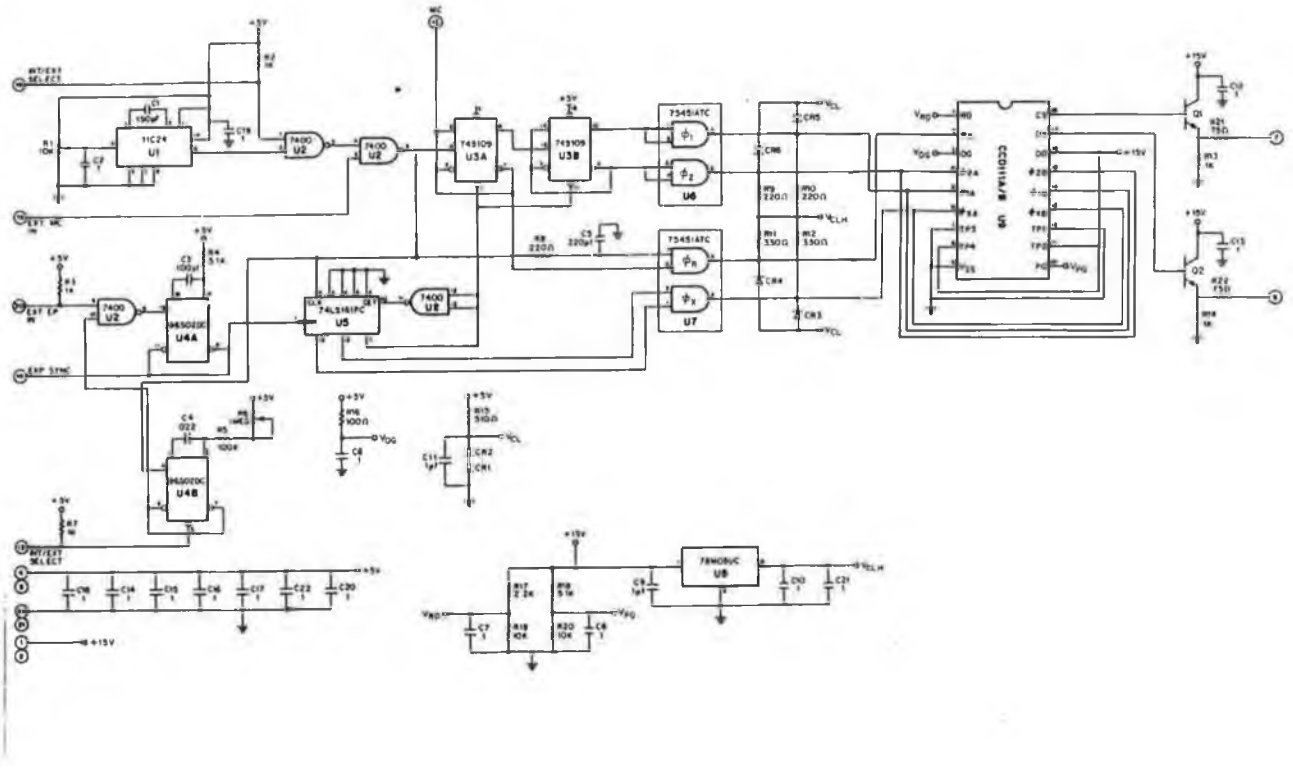

Fig. 12. Circuit diagram of I-SCAN.

Reproduced from CCD 111 Specification.

It was found that bit 3 at pin 11 of the counter pulses 8 clock pulses after the Exposure Sync signal at pin 14 of the board pulses at pin 1, (memory reset), of

the counter. The signal at pin 11 was fed to the R input of the SR flip flop causing Q to reset the NAND gate and enable the signal to the fast counter. At this stage the fast counter and the scan were in sync.

The video output signal from the I-SCAN board was not getting through the input buffer amp at the sample-and-hold amp. The data rate was too fast for a 741 or a 3140 op-amp. These were only useful at frequencies up to 1KHz and 10KHz respectively. An OP42 op-amp was tried and this transmitted a 100KHz square wave through without any distortion. It was found that the video output was riding on an 8V DC level - this is in agreement with manufacturer's specification, and with a gain of x2 on the op amp the signal could not be amplified because the voltage rails for the op amp were at +/-15V. A variable voltage stage was added to the input buffer using a voltage divider circuit to compensate for the 8V DC level.

A chart recorder was then connected to the output buffer, but in order to have the chart recorder on a sensitive voltage scale it was necessary to remove a DC level using another voltage divider. Also, since the function of the sensor was to detect light, not darkness, the signal needed to be inverted. These problems were resolved by adding an inverting summing amplifier with a variable gain and a variable voltage at the summing junction.

The monostable was now causing some problems by giving "echo" pulses after the trigger pulse. I found that the 74LS123 is a level triggered monostable

multivibrator which pulses on a high level. This was replaced with a pin compatible 74LS221, an edge triggered monostable.

The major problem with the Sample-and-Hold circuit at this stage was that the monostable 74221 was still giving echo pulses. Since required pulse duration is approximately 7μs, Cext = 1nF and Rext = 10KΩ. See Fig. 13, '221 Timing/Logic Diagram.

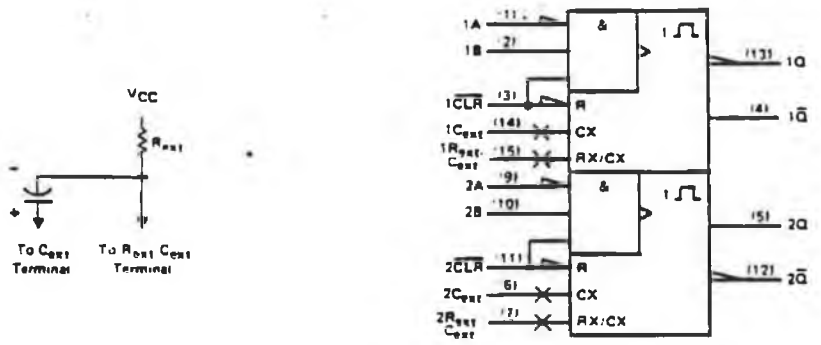

Fig. 13. 74LS221 Timing & Logic.

With the signal fed into the inverting input of the monostable, and with the non inverting input and reset pin tied high, there is noise on the signal at the output of the monostable. The noise is also present at the monostable trigger signal. The noise was traced back to the point where the output of all three comparators are ANDED. Note that since there is no '3 input AND gate' on the S/H circuit board, the monostable trigger pulse is generated from two '2 input AND gates'. The output of the AND gate is 'NANDED' with the Master clock for signal conditioning purposes, and the noise can also be seen at the output of the NAND gate. The noise looks like a pulse moving back through the output of the AND gate at the frequency of the slow clock. To resolve this problem the 555 timer

signal (slow clock) was replaced with a function generator but the result remained the same. The floating inputs of the third comparator were grounded but the noise remained.

At this stage it was discovered that due to the synchronisation being used on the fast clock, the I-SCAN output for any pixel began with the valid video signal followed by the reference information and not vice versa as assumed in Fig. 9b. See also Fig. 7. There is therefore no need to NAND the comparator output with the Master clock signal.

It emerged that the reason for the noise at the output of the comparators is that the CD4040BCN 12 stage binary counters being used in the circuit are ripple counters, i.e. the outputs change in sequential order and that incorrect counts occur briefly during the settling time. The maximum propagation delay reset, T_{phl} with Vcc at 4.5V is 24ns, that is the time between the specified reference points on the input and output voltage waveforms with three state output changing from the defined high level to the defined low level.

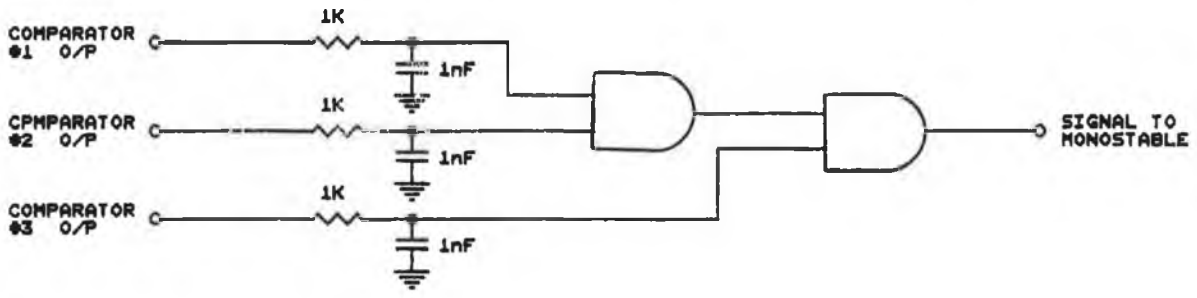

Fig. 14. Time Delay at Output of Comparators.

One solution to the above problem is to delay the outputs of the comparators by a short time before the AND gates to let the signal settle down, thus ensuring that the signals are at the correct values. The time delay used is 1μs. With this modification implemented there remained a small amount of noise from comparator #1, since it is comparing the Least Significant Bits of the counters, the fastest changing bits. This noise is in the form of side band pulses, before and after the delayed output from the comparator. By the addition of a further stage to the output of comparator #1, this noise can be removed.

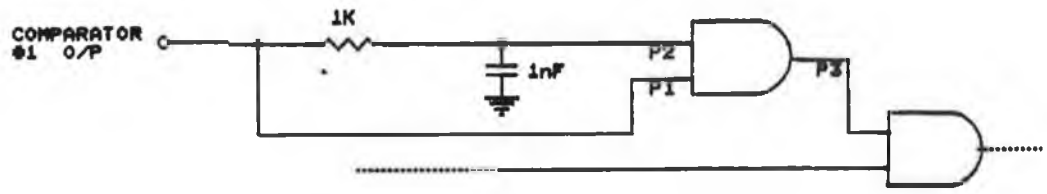

Fig. 15. Additional Delay for Comparator #1.

What is actually happening is the comparator output is being ANDED with the delayed signal so that a clean pulse is fed to the point where the outputs of all three comparators are ANDED.

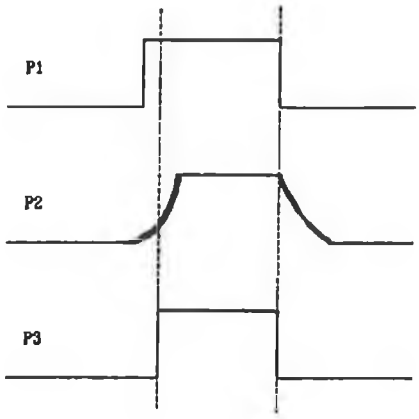

Fig. 16. Comparator #1 Output Timing Diagram.

Now all the noise is removed from the outputs of the comparators and therefore from the input to the monostable.

At the Sample-and-Hold amplifier the output of the buffer read -4V in darkness and between 2V and 4V above this for different intensities of light. An offset of +4V (variable) was added to the output buffer to compensate for this.

Recall, the slow clock is started by a switch. Its counts to 260 and then it is reset using a SR flip flop. The fast clock is started by a pulse from the I-SCAN Board. It counts to 260 and then it is reset. It does not begin again until another scan of the CCD array is about to begin. It takes 260 such scans to build up the image at the output of the Sample-and-Hold circuit. The slow clock is sychronised by the fast clock via a D Type flip flop. This fast clock trigger was replaced by the end of fast scan signal to enhance synchronisation between the clocks.

With the current reset configuration, the information from pixel 1 of the CCD array is being read from the end of one scan until the begin scan switch is pressed. This is due to the fact that the conditioning for the slow clock now comes from count 260 of the fast clock. Specifically, the problem is that at the end of a scan the counters are all reset, the comparators are equal, the monostable input gets a pulse in. The monostable sends a pulse on the falling edge of this high and the Sample-and-Hold amp scans pixel 1. To avoid this problem the system must be configured such that the monostable is disabled in

the time between scans, i.e. that no signal gets to the monostable between scans. The circuit was modified so that an SR flip flop was used to reset the signal to the monostable between scans and allow it to pass during scans.

In Fig. 17 below, S and R are normally high, Q normally low. When R goes low (at the end of one scan), Q goes high and does not allow the signal through the NAND GATE, until S is triggered low (at the beginning of the next scan).

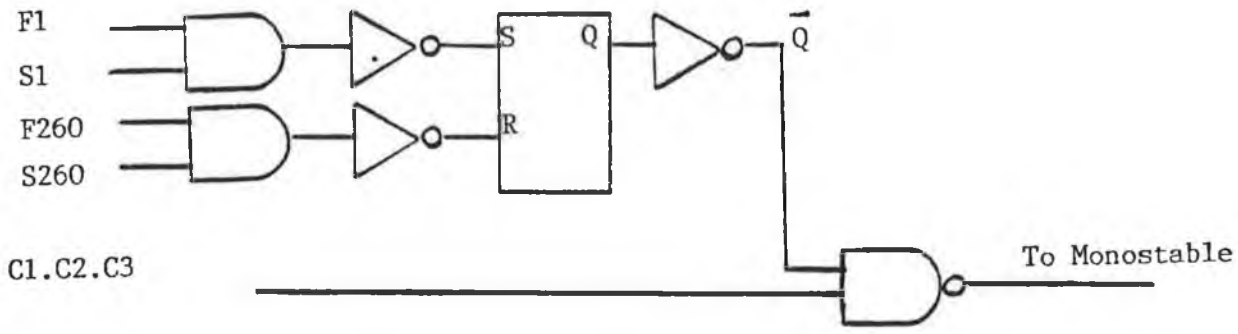

Fig. 17. SR flip flop to Reset the Monostable.

Cx is the output of comparator x. F1 is bit 1 of fast clock. S1 is bit 1 of slow clock etc... The timing diagram for the above circuit is shown in Fig. 18. At this stage the output from the chart recorder was similar to the image directly from the I-SCAN as displayed on the oscilloscope. The output was very noisy since there was a lot of light incident on the CCD array. A large current drain on the +15V supply to the I-SCAN Board (current at 250 mA) was traced to a problem with the regulator 7808. On replacement of the regulator the current was reduced to 100 mA as per the manufacturer's specification.

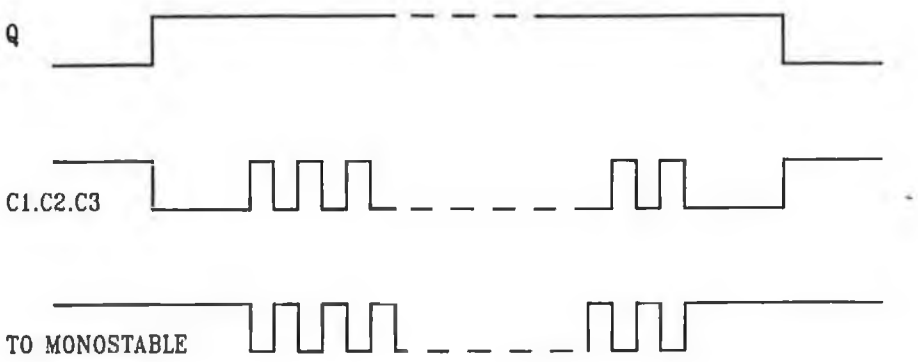

Fig. 18. Timing Diagram for Monostable Reset Circuit.

CIRCUIT ENHANCEMENTS.

AC (hold step) zeroing and DC zeroing stages were added to the Sample-and-Hold amplifier as recommended by manufacturer's specification.

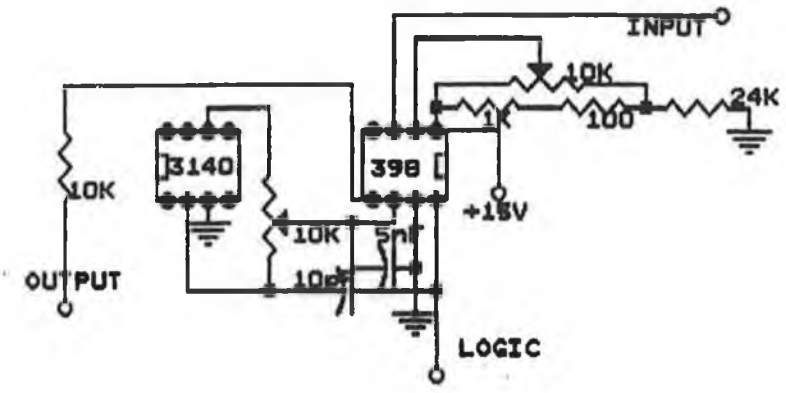

Fig. 19. AC and DC Zeroing on Sample-and-Hold Amp.

Since the Sample-and-Hold amp is sampling the output of the OP42 op-amp a large gain at this stage would cause a larger signal at the input of the Sample-and-Hold amp and therefore a better signal at its output. The feedback resistor (1K) was replaced with 1KΩ + 5KΩ pot in series, with 10KΩ resistor to ground.

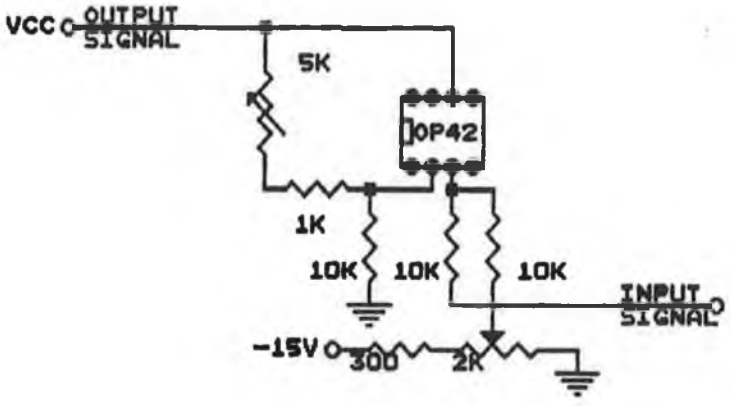

Fig. 20. Modifications to Input Buffer.

The output circuit was examined with a view to changing it to extract the optimum sensitivity information from the signal. At this stage the output circuit was as shown in Fig. 21 below.

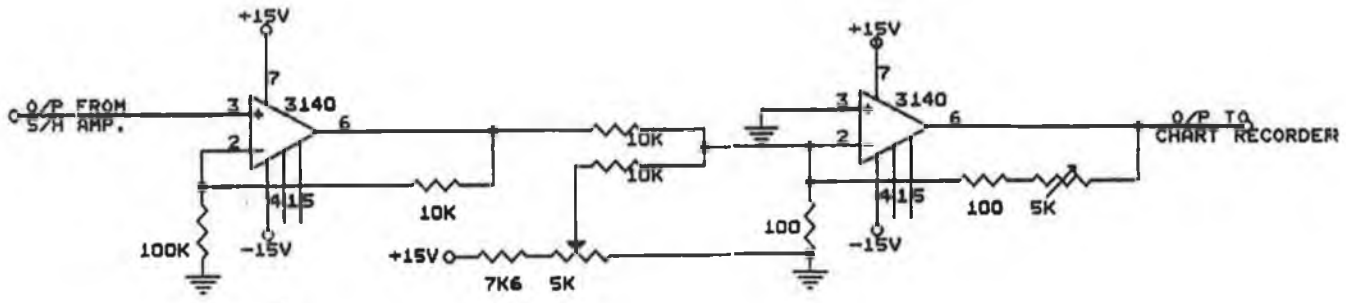

Fig. 21. Output Circuit.

A further enhancement made was to generate the fast clock on board instead of using a function generator. Once generated, the fast clock is fed through a unity gain non inverting op-amp to the I-SCAN Board where its frequency is halved and it becomes the Master clock for both the I-SCAN Board and the Sample-and-Hold circuit board.

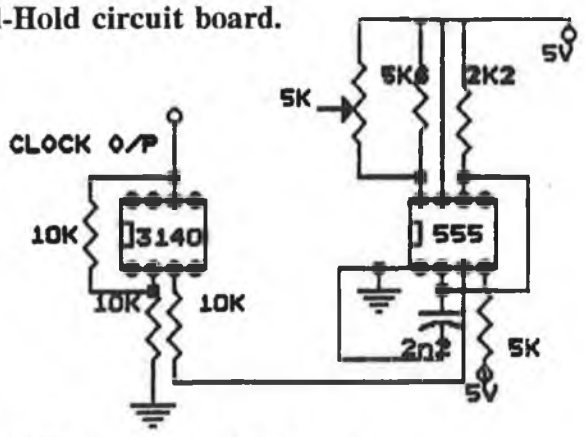

Fig. 22. Fast Clock Circuit.

$$frequency = \frac{1.44}{[R_a + 2R_b]C}$$

C = 2n2 Ra = 2K2 Rb = 5KΩ pot in parallel with 5K6 resistor.

Now we have a variable frequency square wave generator which will generate the required clock frequency of 100 KHz. A power source for a Led was added to the circuit. It was rated at 20mA.

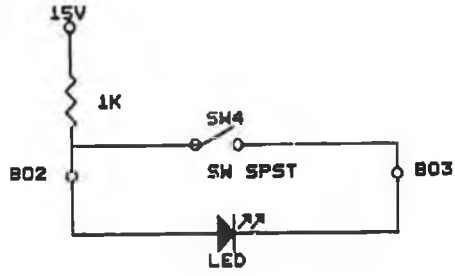

Fig. 23. Led Power Source.

SIGNAL CONDITIONING.

The next major problem was that the Sample-and-Hold amplifier generated an output signal of -12V between scans and thus the intensity information was dwarfed during the scan. One solution to this was to add a compensating positive voltage to the output summing amp between scans but not during scans. To achieve this part of the circuit already in operation, the SR Flip Flop that indicated beginning and end of scan was used.

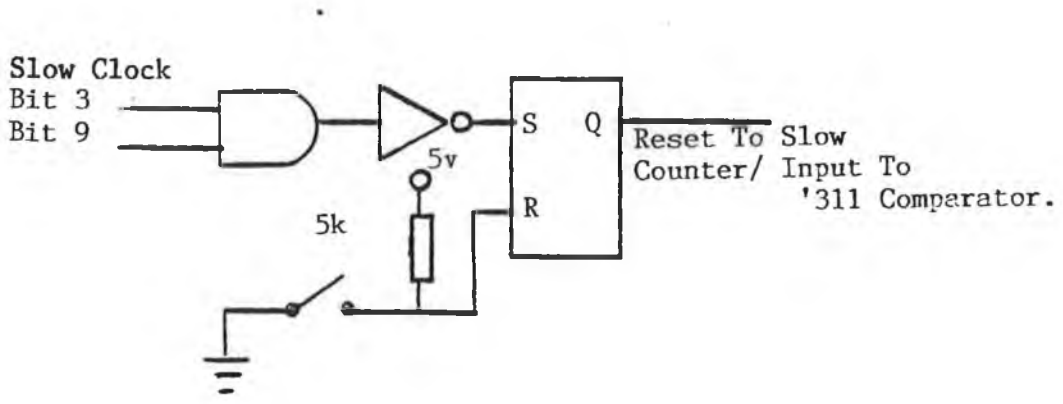

Fig. 24. SR Flip Flop for Comparator Trigger.

The Q signal is used to reset the slow clock. This output switches between +5V (during scans) and 0V (between scans). This signal can be used to switch a voltage on a comparator to different levels depending on the stage of the scan, i.e. we want an output of +12V between scans and 0V during scans. The comparator is a LM311P FET and the setup is displayed in Fig. 26. A pull-up resistor was required to drive the output. A variable resistor was used so that the signal could be adjusted.

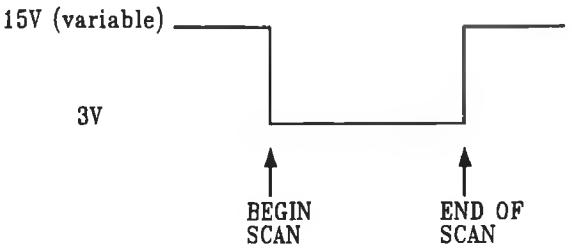

Fig. 25. Output of the Comparator.

At this stage the power rails were set to 0V and +15V. The result was an output of +12V during scans and +3V between scans, See Fig. 25. To ensure that the low level output was set to ground the negative power rail was changed to -3V. Also the inverting input which had been grounded was set to 2.5V so that the input from the Flip Flop was seen as a definite 1 or 0. A voltage follower was added to the output of the comparator. A voltage follower was also added at the output of the Sample-and-Hold amp to prevent its signal being pulled down by the comparator output.

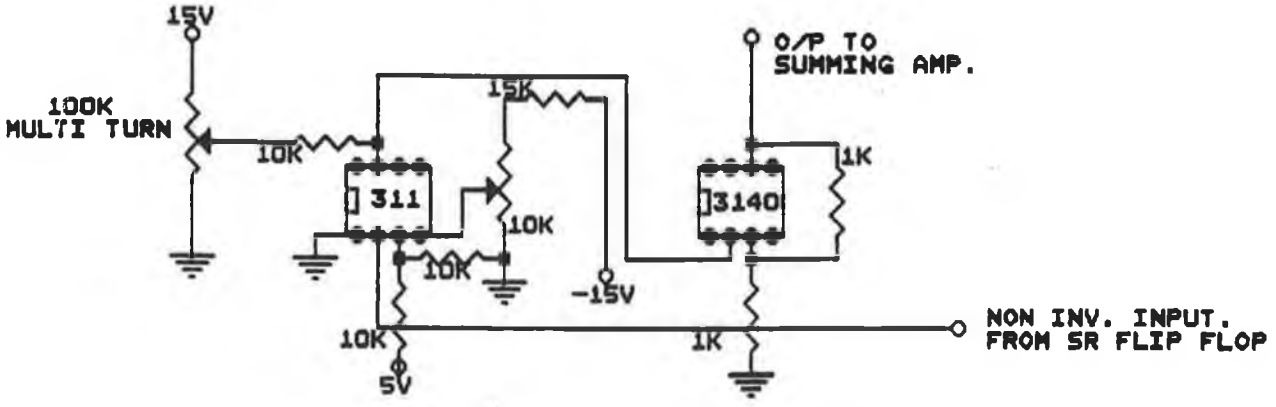

Fig. 26. Comparator Setup.

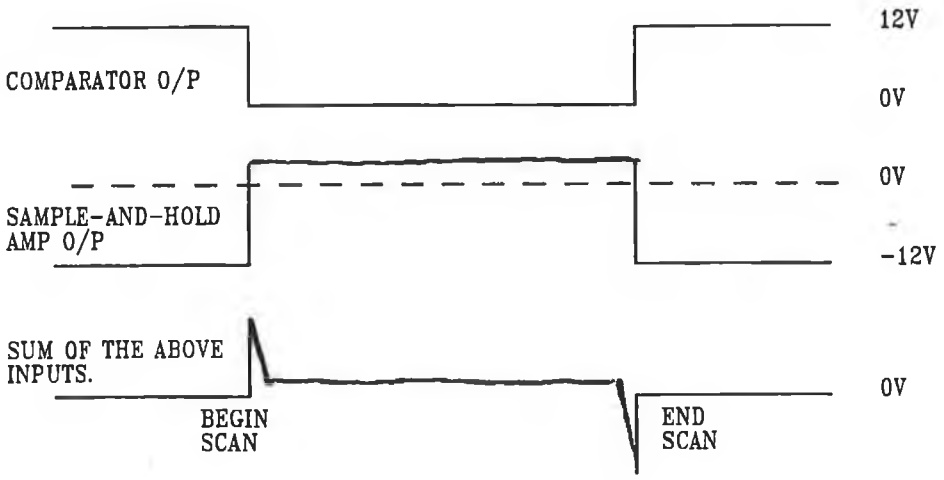

Fig. 27. Timing Diagram for the Output Buffer.

Fig. 27 above displays the outputs of the comparator and the Sample-and-Hold amplifier, and also the output of the summing amplifier. When the signals are summed there is a glitch at the beginning and at the end of the output. These are due to the above signals being slightly out of sync. These glitches can be used as markers for the beginning and end of each scan. Note that when the signal is added to compensate for the -12V level between scans the output of the summing amp is still slightly positive. An additional offset stage (0 - 2V neg variable) was added and the comparator pull-up voltage was adjusted so that there is no offset on the input to the summing amp. The offset mentioned above is small but becomes appreciable at low light levels. To maintain this offset at a low level some changes were made to the output of the Sample-and-Hold amp. The voltage follower mentioned above was changed for an inverting amp with gain of 0.5 followed by an inverting amp with gain of 1. The output circuit is displayed in Fig. 28. The completed circuit diagram is included in Attachment 2.

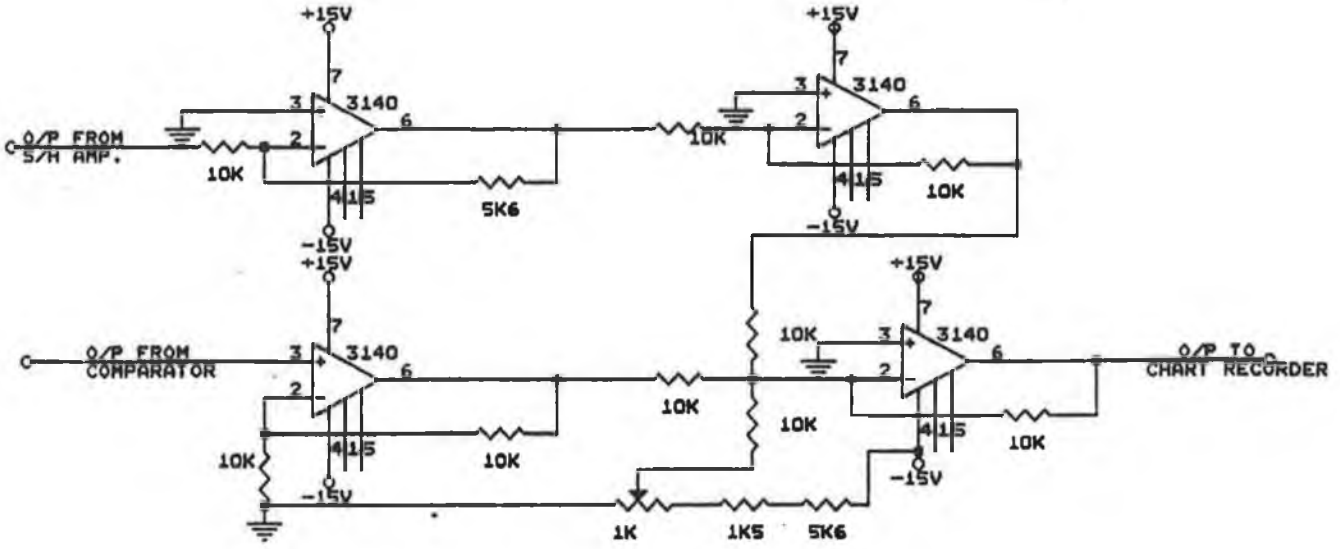

Fig. 28. The Final Output Stage.

Note: There are two voltage adjustments in the circuit to zero the signal for different light levels.

1) **The voltage offset potentiometer at the summing amplifier to adjust the signal during scans.**

2) **The pull-up resistor at the FET to adjust the signal between scans.**

Fig. 29 displays the output of the chart recorder from a sample scan with an illuminated fibre centered over the CCD Array.

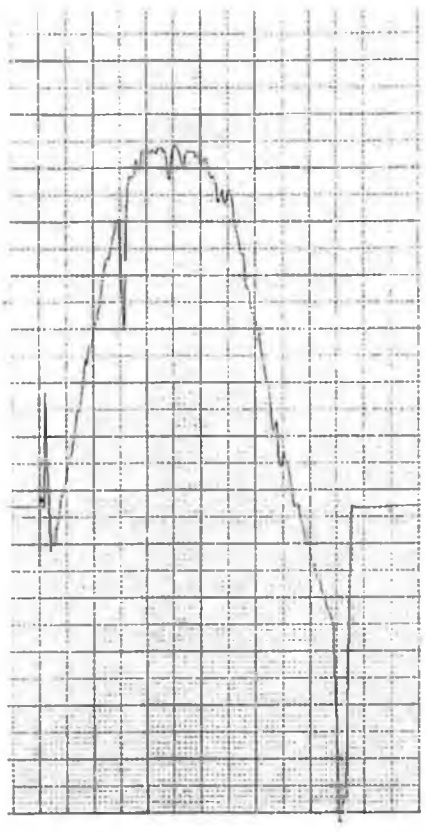

Fig. 29. Chart Recorder Output for a Sample Scan.

CIRCUIT HOUSING & CONNECTION.

Both the I-SCAN Design development board and the CCD signal conditioning circuit board were mounted in diecast boxes. The I-SCAN box, Fig.30, has an adjustible fibre chuck mounted in the lid so that the light from the fibre is incident on the CCD array. The chuck has X, Y & Z adjustments so that the fibre can be aligned properly over the CCD 111 chip on the I-SCAN board. The box has several other connectors:

CX01 I-SCAN SIGNAL OUT (TO OSCILLOSCOPE)

CX02 MASTER CLOCK (CONDITIONED) OUT.

CX03 EXTERNAL MASTER CLOCK IN.

CX04 EXTERNAL EXPOSURE SYNC IN.

D01 15 PIN D CONNECTOR (POWER & SIGNAL CONNECTION FROM S/H CIRCUIT. SEE ATTACHMENT 3.

SW1 EXTERNAL EXPOSURE SYNC ENABLE SWITCH (NORMALLY OFF)

SW2 EXTERNAL MASTER CLOCK ENABLE SWITCH (NORMALLY ON)

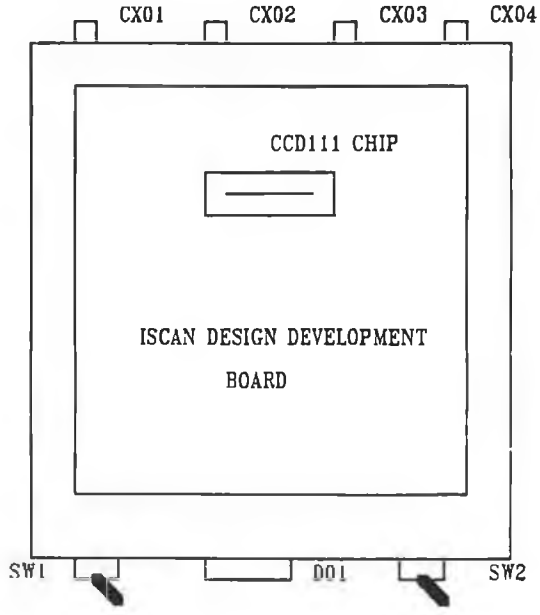

Fig. 30. I-SCAN Circuit.

In the Sample-and-Hold circuit box, Fig. 31,the circuit board is mounted at one side while a power supply for both circuits is mounted at the other side. There is a mains power input connector which has an ON/OFF switch and an overload fuse. The following connectors are mounted on the box:

CX05 OUTPUT TO CHART RECORDER.

CX06 CONDITIONED MASTER CLOCK IN.

CX07 FAST CLOCK OUT.

D02 15 PIN D CONNECTOR TO I-SCAN CIRCUIT. PINOUT AS PER D01.

R37 OFFSET ADJUST.

B01 GROUND. P1 MAINS POWER.

B02 LED + TERMINAL. B03 LED - TERMINAL.

SW3 BEGIN SCAN SWITCH. SW4 LED ON/OFF SWITCH.

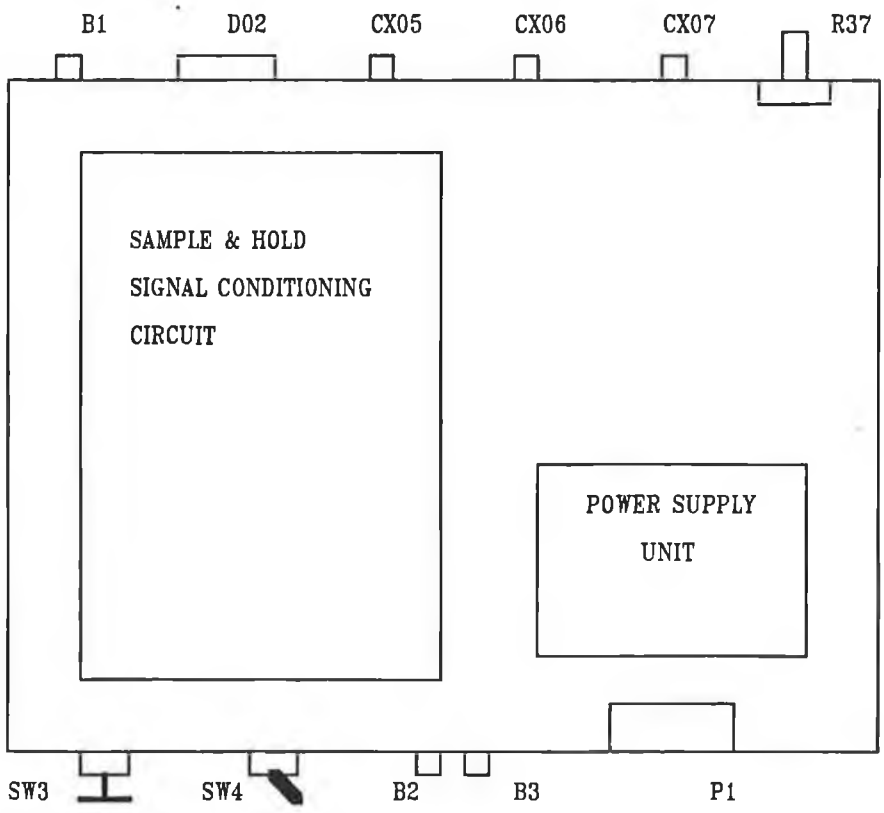

Fig. 31. Sample-and-Hold Signal Conditioning Circuit.

REFERENCES

CHARGE-COUPLED DEVICES AND SYSTEMS.

Edited by M.J. Howes and D.V. Morgan. Wylie 1980.

CHARGE-COUPLED DEVICES: TECHNOLOGY AND APPLICATIONS.

Edited by Roger Melen and Dennis Buss. IEEE Press 1977.

THE ABC OF CCDs.

Walter F. Kosonocky and Donald J. Sauer.

Electron. Des., Vol 23. April 12, 1975.

CHARGE-COUPLED SEMICONDUCTOR DEVICES.

W.S. Boyle and G.E. Smith. Bell Syst. Tech. J., Vol 49. April 1970.

CHARGE-COUPLED DEVICES - AN OVERVIEW.

Walter F. Kosonocky, 1974 Western Electron. Show and Conv. Tech. Papers. Sept 10 - 13, 1974.

IMAGING DEVICES USING THE CHARGE-COUPLED CONCEPT.

David F. Barbe. Proc. IEEE, Vol 63, Jan 1975.

OPTICAL SENSING TECHNIQUES AND SIGNAL PROCESSING.

Tudor E. Jenkins. Prentice Hall, 1987.

ATTACHMENT 1.

THE SAMPLE-AND-HOLD SIGNAL CONDITIONING CIRCUIT DIAGRAM.

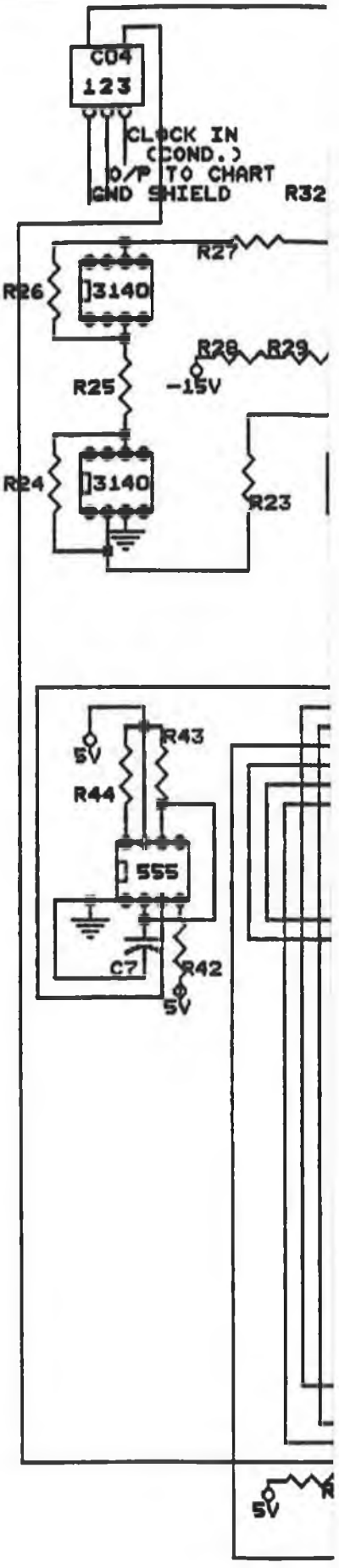
C04
123
CLOCK IN
(COND.)
O/P TO CHART
GND SHIELD
R32
R27
R26
3140
R28
R29
R25
-15V
R24
3140
R23
5V
R43
R44
555
C7
R42
5V
5V

ATTACHMENT 2.

I-SCAN DESIGN DEVELOPMENT BOARD

CCD 111 SENSOR SPECIFICATION.

FAIRCHILD WESTON
Schlumberger
CCD IMAGING DIVISION

CCD Design Development Aids

Fairchild Weston offers printed circuit boards to assist customers in initial experiments with CCD devices. All design development boards do include the sensor and require customer development of optical inputs and processing of the CCD output signal. Design development boards for many devices (CCD 123, 134, 145, 151, and 181) are being engineered for 2nd Quarter 1987 availability.

Fairchild Weston Systems, Inc. CCD Imaging Division
810 W. Maude Ave., Sunnyvale, California 94086
(408) 720-7600, TWX 910-373-2110

FAIRCHILD WESTON
Schlumberger
CCD IMAGING DIVISION

I-SCAN
Design Development Board
CCD111 Sensor

I-SCAN consists of a Fairchild CCD111, 256 element line scan sensor, mounted on a printed circuit card that contains all the necessary CCD111 operating electronics. It is intended for use as a construction aid for experimental systems using CCD line scan sensors or can be incorporated directly into systems requiring 256 elements of resolution. I-SCAN comes fully assembled and tested and requires only the input of power supplies and an oscilloscope to display the video information corresponding to the image placed in front of the sensor.

The I-SCAN card, Figure 1, measures 4½ by 4 inches. The CCD111 is mounted in a socket centrally located on the card. A lens maybe positioned in front of the sensor to focus an image onto the array. All board I/O connections are made through a 22 position single edge card connector with .156 inch center-pacings. The edge connector is compatible with TRW/CINCH type 50-44A-30 or equivalent.

The board circuit, Figure 2, requires a power supply input of +15V at 100mA to Pin 1 and +5V at 200mA to Pin 4. The ground returns should go to Pin 22.

An on-board regulator provides a clock high level voltage of 8V. The +15V supply is divided to achieve a 12V reset drain voltage and a 10V photogate bias voltage required by the CCD111. The output gate voltage, V_{OG} is derived from the +5V* supply.

For normal self-contained operation of the board, Pin 18, the internal/external master clock select line and Pin 12, the internal/external exposure time select are left open.

Voltage controlled oscillator U1 generates a master video clock signal which may be adjusted from approximately 1MHz to 4MHz by potentiometer R1. The frequency of the video clock square wave from U1 is divided by two by flip-flop U3A and one-half of MOS driver U7 amplifies the flip-flop output to provide the ϕR reset clock signal required by the CCD111. The normal amplitude of the ϕR clock signal at the sensor terminal is from a low of about 0.5V to a high of about 8V in accordance with the sensor data sheet recommendations.

The output from U3A is also fed into flip-flop U3B causing another divide by two used in generating the ϕ1 and ϕ2 transport clock signals. The outputs of U3B are fed into MOS driver U6 producing transport clock swings of from a low of about 0.5V to a high of 8.0V. Overall sensor data rate is equal to the ϕ_R clock frequency.

The exposure time of the sensor is controlled internally by one-shot U4B. Length of exposure time is adjusted with R6 giving times > 1mS. To begin an exposure, one shot U4B triggers one-shot U4A; a fast pulse from U4A resets counter U5 and starts it counting. The counting of U5 controls the ϕX transfer pulse through one-half of MOS driver U7. It also stops the transport clocks ϕ1 and ϕ2 during the transfer pulse internal in accordance with CCD111 data sheet recommendations. (See Figure 3.) Note that both transfer clocks ϕ_{XA} and ϕ_{XB} are tied together to achieve a satisfactory transfer.

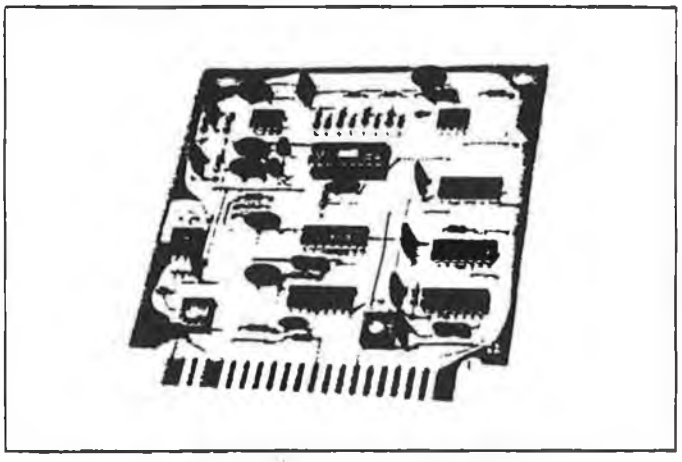

Figure 1 FRONT VIEW

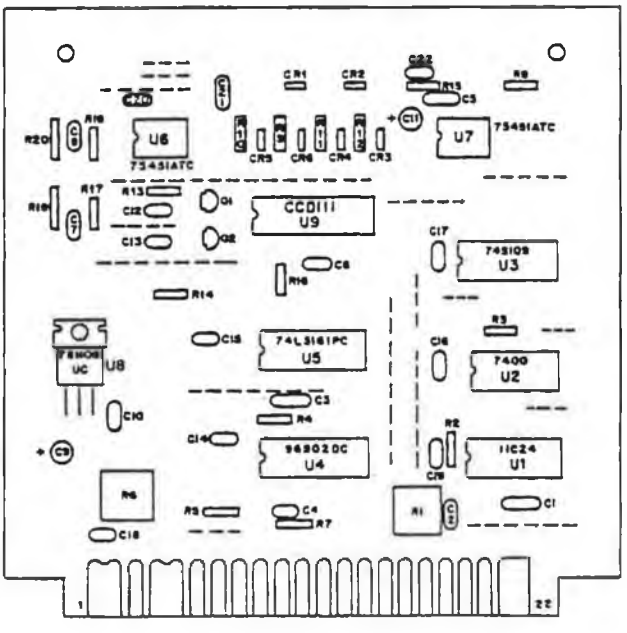

*Adjustment of V_{OG} over the range of 4-7V may be required for optimum operation of the sensor.

NOTICE

This Development Board may not present the optimum test conditions for your design.

Figure 2

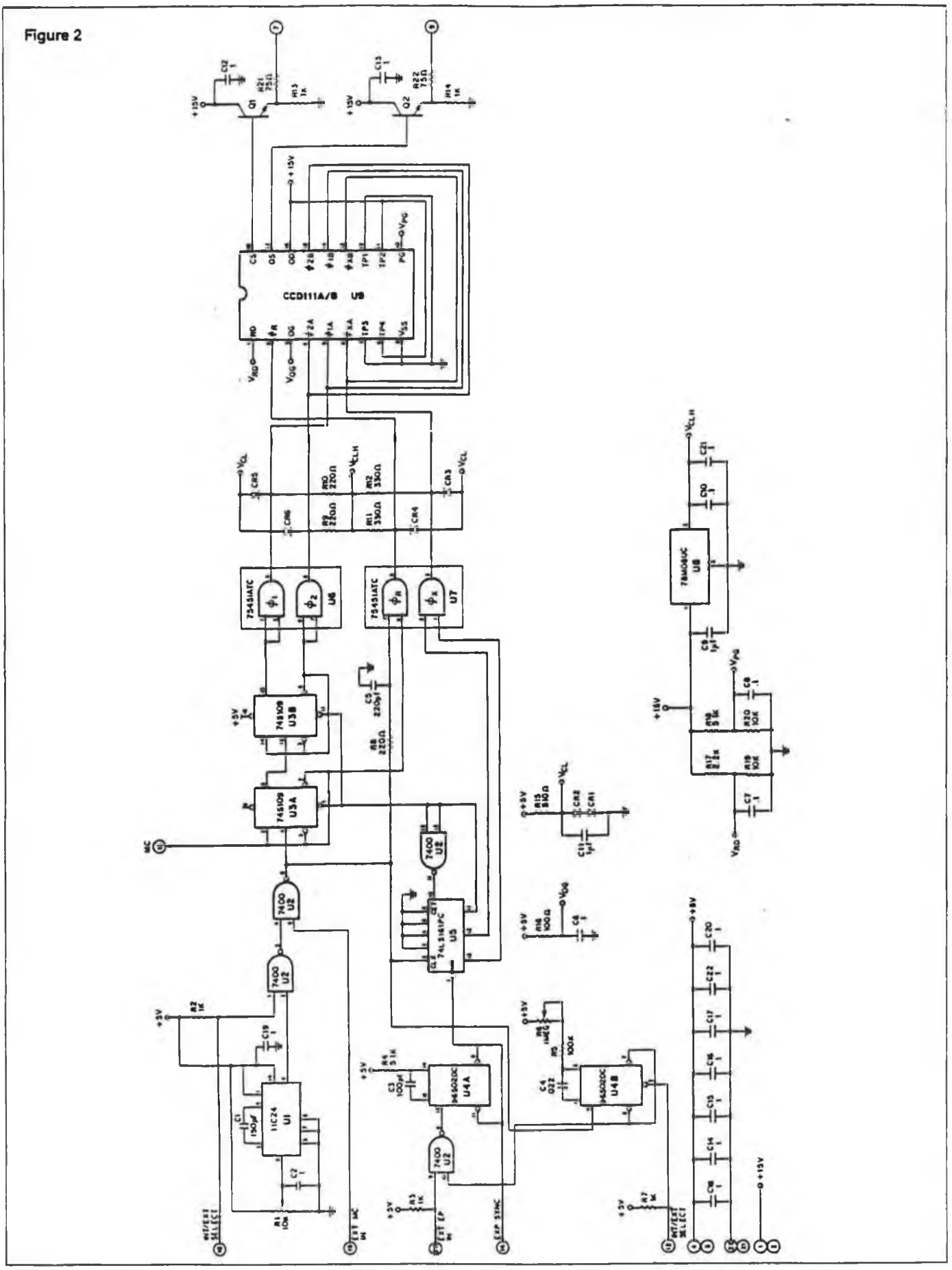
CCD111A/B U8
74S109 U3A
74S109 U3B
7400 U2
74LS161PC U5
74S020C U4A
74S020C U4B
11C24 U1
7545IATC U6
7545IATC U7
7840HDC U8
7400 U6
+15V
+5V
-15V

fter the transfer is completed, counter U5 restarts transport ocks $\phi 1$ and $\phi 2$, and disables itself until its next reset ommand at the start of the next exposure period.

egistors R9-R12 tie the open collector outputs of the MOS rivers to the clock high level voltage and clamp diodes CR3-R6 tied to voltage V_{CL} prevent clock signal excursions below round. Negative clock line transients at the CCD terminals an cause charge-injection which may result in an apparent crease in the dark signal non-uniformity of the sensor.

Pin 18 of the card is held low, an external master clock (TTL evel) may be input on Pin 19. Data rate of the sensor will qual one-half the frequency supplied to Pin 19. If Pin 12 is eld low, the sensor will respond to an external (TTL Level) xposure signal on Pin 20. The exposure signal may be perated asynchronously with the data rate clock. Note in the ming diagram, however, that the $\phi 1$ transport clock signal is the high state at the time of the exposure pulse.

In order not to mix two lines of video information in the transport registers of the CCD, the exposure or integration time of the sensor must be greater than the time necessary to read all the information from the previous line out of the transport registers. (i.e., $t_{INT} > X$ 1
(See Timing Diagram)

Card connector fingers 14 and 15 provide exposure time sync and master clock output signals respectively for external usage; i.e., for synchronizing an oscilloscope for display of the sensor output signals.

The video output and compensation output of the CCD111 sensor are buffered through emitter followers and are made available on connector fingers 9 and 7 respectively. If long co-axial cables are wired to the outputs, the cables should be terminated into 75Ω for best frequency response. The cable terminations will reduce the video signal amplitudes by one-half.

Figure 3 **I-SCAN TIMING DIAGRAM**

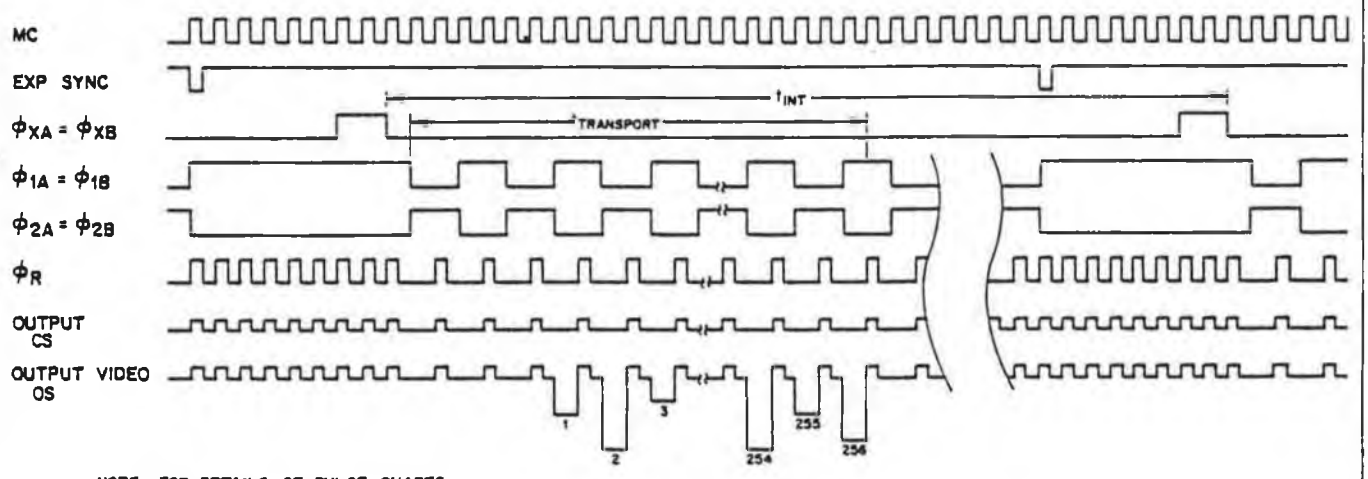

NOTE: FOR DETAILS OF PULSE SHAPES, SEE CCD111 DATA SHEET.

ATTACHMANT 3.

D01 PINOUT.

PINOUT FOR D-CONNECTOR

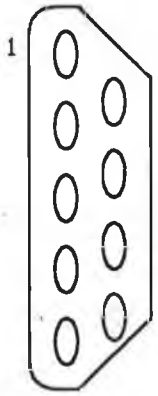

SOCKET

D0101 +15V
D0102 +5V
D0103 RESET TO COUNTER
D0104 NC
D0105 VIDEO OUTPUT
D0106 NC
D0107 NC
D0108 NC
D0109 GROUND

CONNECTORS ON S/H CIRCUIT.

C101 +O/P TO LED
C102 +15V
C103 +5V

C201 VIDEO IN FROM PIN 9 I-SCAN
C202 -15V
C203 GND

C301 CLOCK SYNC. FROM PIN 11 I-SCAN
C302 BEGIN SCAN SWITCH (PIN6 4044 SR FF
C303 GND SIGNAL FOR C302

C401 GND SDIELD FOR C402
C402 O/P TO CHART RECORDER
C403 CLOCK IN (CONDITIONED)

C501 PULL UP RESISTOR R27 TO 311 FET
C502 GND R27
C503 FAST CLOCK OUT (100KHz)

C601 N/C
C602 +15V TO R27
C603 N/C

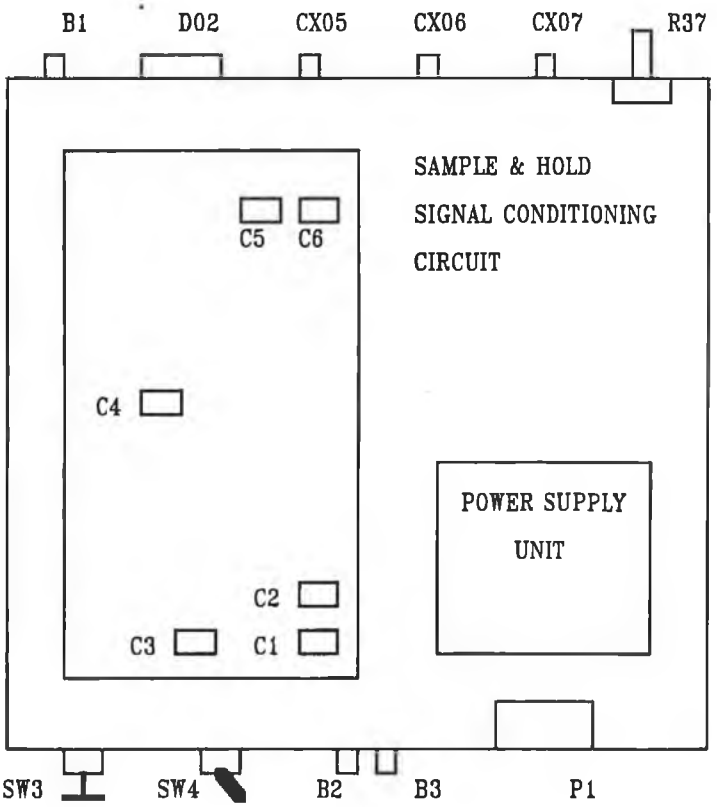

APPENDIX 2

SOFTWARE PROGRAMS.

```
/*************************************************************************/
/*************************************************************************/
/*********                    CENTRE.C                           *********/
/********* Program to calculate the coordinates of the centre    *********/
/********* of a given image.                                     *********/
/*********                    05/02/1992                         *********/
/*************************************************************************/
/*************************************************************************/

#include <stdio.h>
#include <stdlib.h>       /********* Prototyping  *********/
#include <math.h>         /*********     and      *********/
#include <conio.h>        /********* Initialising *********/

#define ROWS        165   /*** (ROWS * COLUMNS) = ROI  ***/
#define COLUMNS     196
#define THRESHOLD    20   /* Intensity value seperating light and dark */

unsigned char store[ROWS][COLUMNS];
unsigned char *start, max1, max2;
char       c, file[15];
FILE       *fptr;
int        corefound, xtotal, x1, x2, ytotal, y1, y2;
float      xdist, ydist;
int        i, j;

float main ()
{

    clrscr ();

    printf ("\n Would you like to find the coordinates of the");
    printf ("\n centre of an image?.....y/n.....");
    c = getchar ();
    while ((c == 'y')  ||  (c == 'Y'))
    {
        /*** Open data file to read in data ***/
        printf ("\n Note : The filename format should be : ________.buf)");
        printf ("\n\n The filename is: .....");
        scanf ("%s", file);
        if ((fptr = fopen(file,"rb")) == NULL)
        {
            printf ("\n Cannot open the file : %s\n",file);
            exit (0);
        }

        /*** Reads in a line of pixel intensities   ***/
        /*** and check along each row to estimate the centre X-coord ***/
        xdist = 0.0;
        xtotal = 0;
        start = &store[0][0];

        for (i=0; i<=ROWS; i++)
        {
            max1 = 0;
```

```
        max2 = 0;
        x1 = 0;
        x2 = 0;
        corefound = 0;
        for (j=0; j<=COLUMNS; j++, start++)
        {

            fread (start, 1, 1, fptr);
            if (corefound)
            {
                if (*start > max2)
                {
                    max2 = *start;
                    x2 = j;
                }
            }
            else
            {
                if (*start > max1)
                {
                    max1 = *start;
                    x1 = j;
                }
            }
            /*** At core of circle ***/
            if ((max1 > THRESHOLD)  &&  (*start < THRESHOLD))
                corefound = 1;
        }

        if (max2 > THRESHOLD)
        {

            xdist = xdist +  ((float) (x1+x2)) / 2.0;
            xtotal = xtotal + 1;

            printf ("\n row %i  %i  %f  %i %i", i, xtotal, xdist, x1, x2);
        }
    }

    /*** X-coordinate of centre ***/
    if (xtotal==0)
    {
        printf ("\n Error - invalid image ");
        printf ("\n Could not find center region along any row");
        printf ("\n    Check value of THRESHOLD for given image ");
        xdist = 0.0;
    }
    else
        xdist = xdist / ((float) xtotal);

    /*** close input buffer ***/
    fclose (fptr);


    /*** loop along each column to estimate the centre Y-coord ***/
```

```
ydist = 0.0;
ytotal = 0;

for (j=0; j<=COLUMNS; j++)
{
    y1 = 0;
    y2 = 0;
    max1 = 0;
    max2 = 0;
    corefound = 0;
    for (i=0; i<=ROWS; i++)
    {
        start = &store[i][j];

        if (corefound)
        {
            if (*start > max2)
            {
                max2 = *start;
                y2 = i;
            }
        }
        else
        {
            if (*start > max1)
            {
                max1 = *start;
                y1 = i;
            }
        }

        /*** At core of circle ***/
        if ((max1 > THRESHOLD)  &&  (*start < THRESHOLD))
        corefound = 1;
    }

    if (max2 > THRESHOLD)
    {
        ydist = ydist +  ((float) (y1+y2)) / 2.0;
        ytotal = ytotal + 1;
        printf ("\n col %i  %i  %f %i %i", j, ytotal, ydist, y1, y2);

    }
}

/*** Y-coordinate of centre ***/
if (ytotal==0)
{

    printf ("\n Error - invalid image.");
    printf ("\n Could not find centre region along any column");
    printf ("\n    Check value of THRESHOLD for given image ");
    ydist = 0.0;
}
else
```

```
            ydist = ydist / ((float) ytotal);

          /*** output results ***/
          printf("\n\n\nThe coordinates of the center of your image");
          printf(" are %4.1f  %4.1f \n", xdist, ydist);

          /*** next image to process ***/
          c = getchar();
          printf("Would you like to process another image?");
          c = getchar();

        }
        return(0);
}
```

```
/*************************************************************************/
/*************************************************************************/
/********* ANALYSE2.C          REV 1.2                 12/1/1993   *********/
/********* Program to calculate the coordinates of the centre of   *********/
/********* a given image, perform an Intensity Vs Radius profile   *********/
/********* of the image, plot the data and write it to a file.     *********/
/*************************************************************************/
/*************************************************************************/

#include <stdio.h>
#include <stdlib.h>       /********* Prototyping  *********/
#include <math.h>         /*********     and      *********/
#include <conio.h>        /********* Initialising *********/
#include <graphics.h>
#include <dos.h>

#define ROWS        165   /*** (ROWS * COLUMNS) = ROI  ***/
#define COLUMNS     196
#define THRESHOLD   70   /* Intensity value seperating light and dark */

unsigned char store[ROWS][COLUMNS];
unsigned char *start, max1, max2;
char      c, file[15];
char      p = 0;
FILE      *fptr,*ifp;
int       corefound, xtotal, x1, x2, ytotal, y1, y2;
float     xdist, ydist;
float     average[60] = {0}, sum[60] ={0};
float     lim1, lim2, maxint;
int       total[60] = {0};
int       i, j, k, maxk, maxx, maxy;
double    radius,a,b,g,d,e,scalex,scaley;
float main ()
{
        int graphdriver=DETECT,graphmode;

        clrscr ();
        printf ("\n Would you like to find the coordinates of the");
        printf ("\n centre of an image?.....y/n.....");
        c = getchar ();
        while ((c == 'y')  ||  (c == 'Y'))
        {
                /*** Open data file to read in data ***/
        printf ("\n Note : Input filename format should be : _______.buf)");
        printf ("\n\n The filename is: .....");
        scanf ("%s", file);
        if ((fptr = fopen(file,"rb")) == NULL)
        {
            printf ("\n Cannot open the file : %s\n",file);
            exit (0);
        }
        printf ("\n Note : Output filename format should be : _______.dat)");
        printf ("\n\n The filename is: .....");
        scanf ("%s", file);
        if ((ifp = fopen(file,"w+")) == NULL)
```

```
{
    printf ("\n Cannot open the file : %s\n",file);
    exit (0);
}


/*** Reads in a line of pixel intensities   ***/
/*** and check along each row to estimate the centre X-coord ***/
xdist = 0.0;
xtotal = 0;
start = &store[0][0];

for (i=0; i<=ROWS; i++)
{
    max1 = 0;
    max2 = 0;
    x1 = 0;
    x2 = 0;
    corefound = 0;
    for (j=0; j<=COLUMNS; j++, start++)
    {

        fread (start, 1, 1, fptr);
        if (corefound)
        {
            if (*start > max2)
            {
                max2 = *start;
                x2 = j;
            }
        }
        else
        {
            if (*start > max1)
            {
                max1 = *start;
                x1 = j;
            }
        }
        /*** At core of circle ***/
        if ((max1 > THRESHOLD)  &&  (*start < THRESHOLD))
            corefound = 1;
    }

    if (max2 > THRESHOLD)
    {

        xdist = xdist +  ((float) (x1+x2)) / 2.0;
        xtotal = xtotal + 1;

        printf ("\n row %i  %i  %f  %i %i", i, xtotal, xdist, x1, x2);
    }
}
```

```
/*** X-coordinate of centre ***/
if (xtotal==0)
{
    printf ("\n Error - invalid image ");
    printf ("\n Could not find center region along any row");
    printf ("\n    Check value of THRESHOLD for given image ");
    xdist = 0.0;
}
else
    xdist = xdist / ((float) xtotal);

/*** close input buffer ***/
fclose (fptr);


/*** loop along each column to estimate the centre Y-coord ***/
ydist = 0.0;
ytotal = 0;

for (j=0; j<=COLUMNS; j++)
{
                y1 = 0;
                y2 = 0;
                max1 = 0;
                max2 = 0;
                corefound = 0;
                for (i=0; i<=ROWS; i++)
                {
                        start = &store[i][j];

                        if (corefound)
                        {
                                if (*start > max2)
                                {
                                        max2 = *start;
                                        y2 = i;
                                }
                        }
                        else
                        {
                                if (*start > max1)
                                {
                                        max1 = *start;
                                        y1 = i;
                                }
                        }

        /*** At core of circle ***/
        if ((max1 > THRESHOLD)  &&  (*start < THRESHOLD))
        corefound = 1;
    }

    if (max2 > THRESHOLD)
    {
        ydist = ydist +  ((float) (y1+y2)) / 2.0;
```

```
        ytotal = ytotal + 1;
        printf ("\n col %i  %i  %f %i %i", j, ytotal, ydist, y1, y2);
                        }
          }

/*** Y-coordinate of centre ***/
if (ytotal==0)
{
                        printf ("\n Error - invalid image.");
    printf ("\n Could not find centre region along any column");
    printf ("\n    Check value of THRESHOLD for given image ");
    ydist = 0.0;
}
else
    ydist = ydist / ((float) ytotal);

/*** output results ***/
printf("\n\n\nThe coordinates of the center of your image");
printf(" are %4.1f  %4.1f \n", xdist, ydist);

 /*** Intensity profile of the image ***/

for(i = 0; i <= ROWS; i++)
{
                for(j = 0; j <= COLUMNS; j++, start++)
        {
                fread(start,1,1,fptr);  /** Reads in a line of  **/

        }
}
fclose(fptr);
start = &store[0][0];
for(i = 0; i <= ROWS; i++)
{
  printf("\nProgram is running, Pass %i\n",i);
  for(j = 0; j <= COLUMNS; j++, start++)
  {
                a = i - ydist;
                b = pow(a,2);
                g = j - xdist;
                d = pow(g,2);
                e = b + d;
                radius = sqrt(e);
                for(k = 1; k < 50; k++)
                {
                        lim1 = 3.0*(k - 1);
                        lim2 = 3.0*k;
                        if((radius > lim1) && (radius < lim2))
                        {
                        sum[k] = sum[k] + store[i][j];
                        total[k] = total[k] + 1;
                        }
                }
        }
}
```

```
        for(k = 1; k < 50; k++)
                {
                        if(total[k] == 0)
                        {
                                average[k] = 0;
                        }
                        else
                        {
                                average[k] = sum[k]/total[k];
                        }
                }
                initgraph(&graphdriver,&graphmode,"d:\\tc\\bgi\\");
                setbkcolor(EGA_DARKGRAY);
                setcolor(EGA_YELLOW);

                printf("\n\t\t\t\t\txdist = %f\n\t\t\t\t\tydist =%f \n",xdist,

                maxint = 0.0;

                for(k=1;k<50;k++)
                {
                        if(average[k]>maxint) maxint=average[k];
                }

                maxk=50;
                k=50;
                while(average[k]==0.0)
                {
                        maxk=k;
                        k--;
                }
                printf("\t\t\t\t\tmax k == %d\n\t\t\t\t\tmax average == %f",k,
                getch();
                maxx=getmaxx();
                maxy=getmaxy();
                scalex=maxx/maxk;
                scaley=maxy/maxint;

                moveto(0,0);
                lineto(0,maxy);
                lineto(maxx,maxy);
                moveto(0,maxy-(average[1]*scaley));
                for(k = 1; k < 50; k++)
                {
                        lineto(k*scalex,maxy-(average[k]*scaley));
                        fprintf(ifp,"%f\n",average[k]);
                }
                getch();
                printf("\nWould you like to profile another image?");
                fclose(ifp);
                c='';
                while ((c!='y')&&(c!='Y')&&(c!='n')&&(c!='N')) c=getchar();
                closegraph();
        }
        return(0);

}
```

```
 /*****************************************************************/
/*****************************************************************/
/*******  HALFPOW.C                                VERSION 2.0  *******/
/*******  PROGRAM TO READ IN VALUES FROM A DATA FILE, NUMBER *******/
/*******  THE ENTRIES FROM 1 TO 49, FIND THE MAXIMUM VALUE,  *******/
/*******  MAX INTENSITY, AND NORMALIZE SO THAT I(max) = 1.   *******/
/*******  THEN FIND THE LOCATIONS OF THE HALF POWER POINTS   *******/
/*******  AT EITHER SIDE AND PRINT THE RESULTS TO FILE.      *******/
/*****************************************************************/
/*****************************************************************/

#include <stdio.h>
#include <math.h>
#define ARRAY 49

void main();

FILE *in1file,*in2file,*in3file,*in4file,*out1file,*out2file;
FILE *INFILE,*OUTFILE;

void main()

{
        float k,l,x,y,z,MAX;
        float LHS=999.0;
        float RHS=999.0;
        int HPL=999;
        int HPR=999;
        int a=1;
        int b=1;
        int j,AT;

        INFILE=fopen("y0na2a.dat","r");
        in1file=INFILE;
        in2file=INFILE;
        in3file=INFILE;
        in4file=INFILE;
        out1file=fopen("ha0na2a.dat","w");
        out2file=fopen("hb0na2a.dat","w");

        for(j=1;j<=ARRAY;j++)
        {
                fscanf(in1file,"%f",&k);            /* FINDING MAXIMUM VALUE *
                if(k>MAX)                           /* OF INTENSITY          *
                {
                        MAX = k;
                        AT = j;
                }
        }

        for(j=1;j<=ARRAY;j++)
        {
                y=l/MAX;
                fscanf(in2file,"%f",&l);             /*NORMALIZING SO THAT  */
        /*      fprintf(out1file,"%d\t%f\t%f\n",j,l,y);MAX INTENSITY VALUE=1*/
```

```
        }

        for(a=1;a<AT;a++)
        {
                fscanf(in3file,"%f",&l);
                printf("%f\t",l);                       /*FINDING THE LHS HALF*/
                y=l/MAX;                                /*POWER LOCATION      */
                printf("%f\t",y);
                if(y<0.6)
                {
                        x=(y-0.5)*(y-0.5);
                        z=sqrt(x);
                        if(z<LHS)
                        {
                                LHS=z;
                                HPL=a;
                        }
                }
        }

        for(b=1;b<ARRAY;b++)
        {
                fscanf(in4file,"%f",&l);
                if(b>AT)
                {                                       /*FINDING THE RHS HALF*/
                        printf("%f\t",l);                    /*POWER LOCATION
                        y=l/MAX;
                        printf("%f\t",y);
                        if(y<0.6)
                        {
                                x=(y-0.5)*(y-0.5);
                                z=sqrt(x);
                                if(z<RHS)
                                {
                                        RHS=z;
                                        HPR=b;
                                }
                        }
                }
        }

        fprintf(stdout,"Max intensity = %f\n",MAX);
        fprintf(stdout,"Occurred at row %d\n",AT);
        fprintf(stdout,"Half power point LHS = %d\n",HPL);
        fprintf(stdout,"Half power point RHS = %d\n",HPR);
        fprintf(stdout,"Note:  999 indicates no valid entry");
    fclose(INFILE);
        fclose(in1file);
        fclose(in2file);
        fclose(in3file);
        fclose(in4file);
        fclose(out1file);
        fclose(out2file);
}
```